PL-TR--
95-1033

EXPERIMENTAL STUDY OF NONLINEAR PERIODIC STRUCTURES

Michelle S. Malcuit
Christopher Herbert
Christy Heid

Department of Physics
16 Memorial Drive East
Lehigh University
Bethlehem, PA 18015

May 1995

Final Report

PHILLIPS LABORATORY
Lasers and Imaging Directorate
AIR FORCE MATERIEL COMMAND
KIRTLAND AIR FORCE BASE, NM 87117-5776

PL-TR--95-1033

This final report was prepared by the Lehigh University, Depatment of Physics, 16 Memorial Drive, Bethlehem, PA 18015 under Contract F29601-91-K-0082, Job Order 33260707 with the Phillips Laboratory, Kirtland Air Force Base, New Mexico. The Laboratory Project Officer-in-Charge was Christopher M. Clayton (LIDN).

When Government drawings, specifications, or other data are used for any purpose other than in connection with a definitely Government-related procurement, the United States Government incurs no responsibility or any obligation whatsoever. The fact that the Government may have formulated or in any way supplied the said drawings, specifications, or other data, is not to be regarded by implication, or otherwise in any manner construed, as licensing the holder, or any other person or corporation; or as conveying any rights or permission to manufacture, use, or sell any patented invention that may in any way be related thereto.

This report has been authored by a contractor of the United States Government. Accordingly, the United States Government retains a nonexclusive, royalty-free license to publish or reproduce the material contained herein, or allow others to do so, for the United States Government purposes.

This report has been reviewed by the Public Affairs Office and is releasable to the National Technical Information Service (NTIS). At NTIS, it will be available to the general public, including foreign nationals.

If your address has changed, if you wish to be removed from the mailing list, or if your organization no longer employs the addressee, please notify PL/LIDN, 3550 Aberdeen Ave SE, Kirtland AFB, NM 87117-5776, to help maintain a current mailing list.

This report has been reviewed and is approved for publication.

Christopher M. Clayton

CHRISTOPHER M. CLAYTON
Project Officer

FOR THE COMMANDER

Marc R Hallada

MARC R. HALLADA
Lt Col, USAF
Chief, Laser Systems Division

Lanny V. Larson

LANNY V. LARSON
Col, USAF
Director, Lasers and Imaging Directorate

DO NOT RETURN COPIES OF THIS REPORT UNLESS CONTRACTUAL OBLIGATIONS OR NOTICE ON A SPECIFIC DOCUMENT REQUIRES THAT IT BE RETURNED.

REPORT DOCUMENTATION PAGE

Form Approved
OMB No. 0704-0188

1. AGENCY USE ONLY (Leave blank)	2. REPORT DATE	3. REPORT TYPE AND DATES COVERED
	May 1995	Final Report: Aug 91 - Apr 95

4. TITLE AND SUBTITLE

Experimental Study of Nonlinear Periodic Structures

5. FUNDING NUMBERS

C: F29601-91-K-0082
PE: 62601F
PR: 3326
TA: 07
WU: 07

6. AUTHOR(S)

Michelle S. Malcuit
Christopher Herbert
Christy Heid

7. PERFORMING ORGANIZATION NAME(S) AND ADDRESS(ES)

Department of Physics
16 Memorial Drive East
Lehigh University
Bethlehem, PA 18015

8. PERFORMING ORGANIZATION REPORT NUMBER

9. SPONSORING/MONITORING AGENCY NAME(S) AND ADDRESS(ES)

Phillips Laboratory/LI
3550 Aberdeen Ave SE
Kirtland AFB, NM 87117-5776

10. SPONSORING/MONITORING AGENCY REPORT NUMBER

PL-TR--95-1033

11. SUPPLEMENTARY NOTES

12a. DISTRIBUTION/AVAILABILITY STATEMENT

Approved for public release;
distribution unlimited.

12b. DISTRIBUTION CODE

13. ABSTRACT *(Maximum 200 words)*

The optical properties of two examples of nonlinear periodic structures experimentally studied: colloidal crystals used as nonlinear distributed feedback structures and nonlinear volume holographic elements. The transmission of the colloidal crystals was found to be dramatically modified by an incident field whose frequency was tuned within or near the stop gap of the crystal. Optical limiting was observed when the frequency of the incident field was tuned to the high frequency edge of the stop gap. Optical switching and bistability were observed when the frequency was tuned to within the stop gap. The switching intensity was seen to decrease as the frequency of the incident light was tuned further into the stop gap. This result can not be explained by the simple model of a nonlinear distributed feedback structure. The transmission was also found to exhibit temporal fluctuations at high intensities. The nonlinear volume holographic structures consisted of a porous photopolymer in which a permanent grating was recorded and then was imbibed with a nematic liquid crystal. The diffraction efficiency of the grating was switched from high to low using a control beam power of 8.4 mW. The response time of the switching was limited by the response time of the thermal nonlinearity of the liquid crystal and was measured to be approximately 1 ms.

14. SUBJECT TERMS

nonlinear periodic stuctures, optical switching, bistability, optical limiting, colloidal crystals, distributed optical feedback, volume hologram

15. NUMBER OF PAGES

68

16. PRICE CODE

17. SECURITY CLASSIFICATION OF REPORT	18. SECURITY CLASSIFICATION OF THIS PAGE	19. SECURITY CLASSIFICATION OF ABSTRACT	20. LIMITATION OF ABSTRACT
UNCLASSIFIED	UNCLASSIFIED	UNCLASSIFIED	SAR

Table of Contents

List of Figures

Abstract

In this work we have studied experimentally the optical properties of two examples of nonlinear periodic structures: colloidal crystals used as nonlinear distributed feedback structures and nonlinear volume holographic elements. The transmission of the colloidal crystals was found to be dramatically modified by an incident field whose frequency was tuned within or near the stop gap of the crystal. Optical limiting was observed when the frequency of the incident field was tuned to the high frequency edge of the stop gap. Optical switching and bistability were observed when the frequency was tuned to within the stop gap. The switching intensity was seen to decrease as the frequency of the incident light was tuned further into the stop gap. This result can not be explained by the simple model of a nonlinear distributed feedback structure. The transmission was also found to exhibit temporal fluctuations at high intensities. The nonlinear volume holographic structures consisted of a porous photopolymer in which a permanent grating was recorded and then was imbibed with a nematic liquid crystal. The diffraction efficiency of the grating was switched from high to low using a control beam power of 8.4 mW. The response time of the switching was limited by the response time of the thermal nonlinearity of the liquid crystal and was measured to be approximately 1 ms.

I. Introduction

In this report we present results of our experimental investigation of nonlinear periodic structures. The properties of linear periodic structures and the theoretical predictions for the optical properties of nonlinear periodic structures are reviewed first as an introduction. Our measurements of the optical properties of nonlinear distributed feedback structures formed from colloidal crystals are then presented. The properties of nonlinear volume holographic gratings formed from a liquid crystal/porous photopolymer composite are then discussed and the results of an optical switching experiment are presented. Publications resulting from this work are found in Refs. [1-4].

Periodic dielectric structures have been used for some time as interference filters, dielectric mirrors and antireflection coatings because of their selective transmission and reflection properties. Distributed feedback structures (DFBS) are periodic structures that consist of a large number of alternating layers of high and low dielectric constant with light propagating in the direction of the refractive index variation. The small difference in refractive index between successive layers leads to a very narrow band of frequencies for which the structure is highly reflective. This band of frequencies is commonly referred to as a stop gap or stop band. The central frequency of the stop gap corresponds to the condition where the wavelength of the light inside the structure is equal to one half the period of the dielectric layers. This condition is known as the Bragg resonance.

Recently there has been a great deal of interest in the optical properties of period dielectric structures with a large intensity dependent index of refraction. For the case of distributed feedback structures when the frequency of the incident light is tuned to a frequency near or inside the stop gap, theoretical studies have predicted the transmission to exhibit optical power limiting, optical bistability [5-9], self pulsing, chaos [10-13], and soliton formation [14-19]. For the case of transmission gratings theoretical studies predict a modification of the diffraction efficiency of the structure in the presence of the high intensity field. This modification can be used for degenerate two-beam coupling [20]. In our experimental study we have investigated these effects using two different material systems. We have studied colloidal crystals as a nonlinear distributed

feedback system and have studied composite gratings formed using a porous photopolymer and a nematic liquid crystal as switchable gratings [4].

I.A. Linear Periodic Structures

In this work we have been interested in the propagation of light though nonlinear periodic structures. To begin the discussion we will first briefly review the optical properties of periodic structures whose index of refraction is not intensity dependent. A periodic structure is a material whose index of refraction varies spatially throughout the structure. We have studied both the transmission geometry and distributed feedback geometry in this work. For the case of the distributed feedback geometry, the index variation is along the direction of propagation of the light. For the transmission geometry the index variation is perpendicular to the direction of propagation. We will first limit the discussion to the specific case of the distributed feedback geometry.

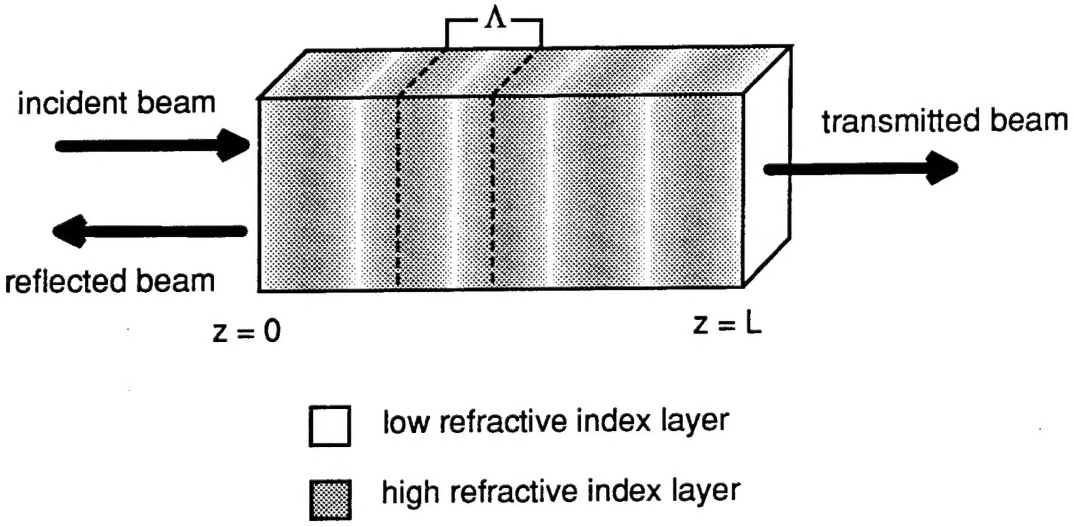

Figure 1. *Schematic diagram of a distributed feedback structure.*

Consider a DFBS with a spatial period for the index variation that is comparable to the wavelength of light. Figure 1 is a schematic diagram of the DFBS. The index variation can be written as

$$n(z) = n_o + n_1 \cos(2\beta_o z) \qquad (1)$$

where n_o is the average index of refraction and n_1 is the index modulation that is responsible for the coupling between forward- and backward-propagating fields in the structure. The quantity $\beta_o = n_o\pi/\Lambda$ is the spatial frequency of the index modulation where Λ is the spatial period of the index modulation. For this type of structure, certain frequencies of light will not be allowed to freely propagate.

To calculate the transmission, the coupled amplitude equations describing the propagation of light through the structure can be solved. Assume that the field inside the periodic structure can be written as

$$E(z,t) = \left[A(z)e^{i\beta z} + B(z)e^{-i\beta z}\right]e^{-i\omega t} + c.c. \tag{2}$$

where A(z) and B(z) are the amplitudes of the forward- and backward-propagating fields, respectively. If the slowly varying amplitude approximation is made and only phase matched terms are kept the coupled amplitude equations can be written as [21]

$$\frac{dA}{dz} = i\kappa Be^{-i\Delta\beta z} \tag{3a}$$

$$\frac{dB}{dz} = -i\kappa Ae^{i\Delta\beta z} \tag{3b}$$

where $\kappa = \beta_o n_1/2n_o$ is the coupling constant and $\Delta\beta = \beta - \beta_o$ is the detuning of the frequency of the incident light from Bragg resonance. These equations have been solved analytically [21,22]. The predicted transmission of a DFBS of length L and κL=3.0 is shown in Fig. 2. The region of low transmission is often referred to as the stop gap. The stop gap is centered at $\Delta\beta L = 0$.

The transmission of a DFBS is strongly dependent on the coupling constant κL. Figures 3a and 3b show the transmission of DFBS with κL=1 and 2, respectively. From these figures we see that the transmission at Bragg resonance ($\Delta\beta = 0$) decreases with increasing coupling strength and

width of the stop gap increases with increased coupling strength. The width of the stop gap can be found to be

$$\Delta\omega_{gap} = \frac{\kappa n_o}{2c}. \tag{4}$$

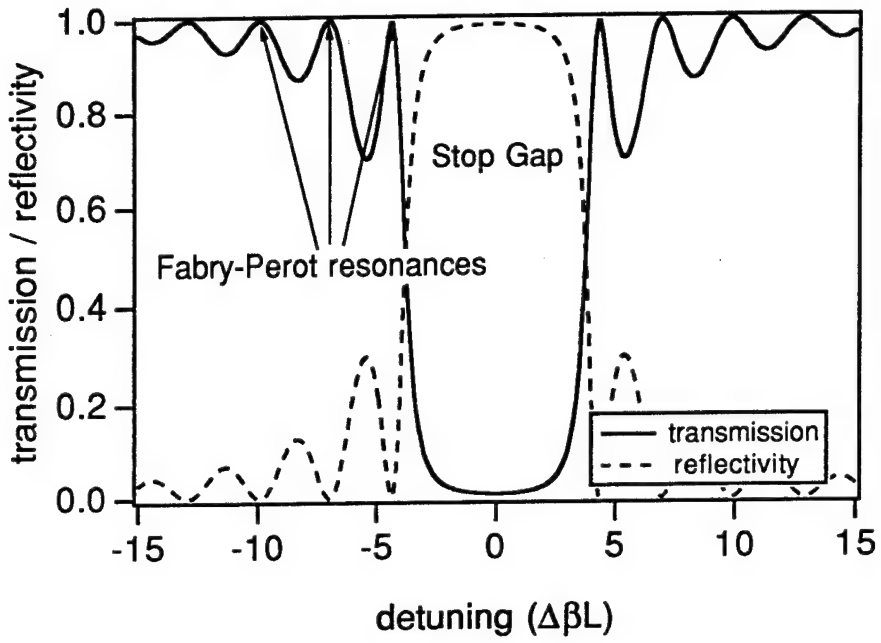

Figure 2. *The transmission and reflectivity plotted as a function of detuning for a DFBS with a* $\kappa L=3.0$

I.B. Nonlinear Periodic Structures

The transmission of DFBS whose index of refraction is intensity dependent is predicted to exhibit optical limiting , optical bistability [5-9], and self pulsing [10-13]. These theoretical predictions will be reviewed briefly in this section.

In the previous section it was assumed that the index of refraction of the DFBS was not dependent on the local field inside the structure. We are now interested in how the transmission of such a structure is modified when the spatially varying index of refraction is assumed to be intensity dependent. We assume that the index of refraction can be written as

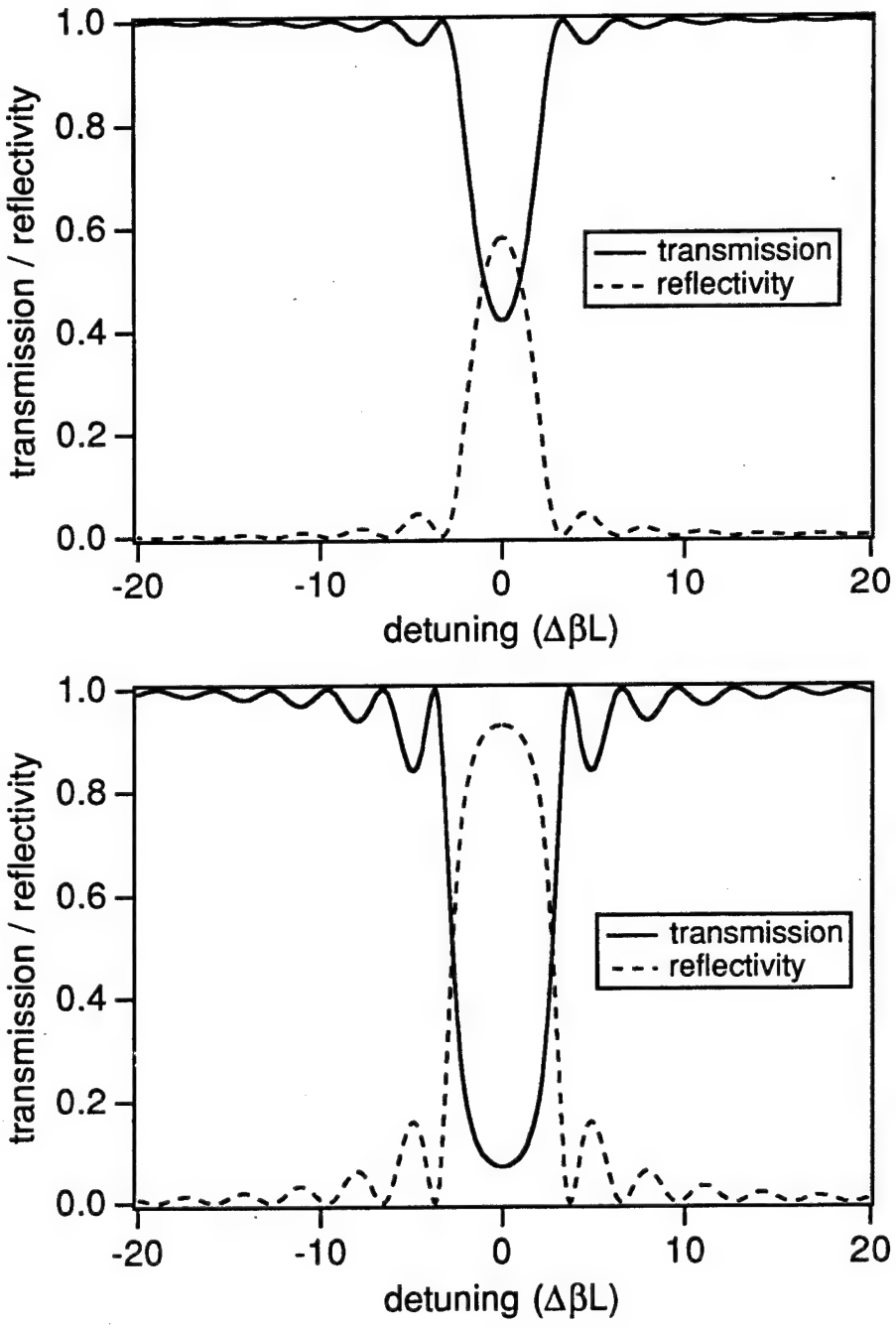

Figure 3. *The transmission and reflectivity plotted as a function of detuning for a DFBS with (a) $\kappa L=1.0$ and (b) $\kappa L=2.0$.*

$$n(z) = n_o + n_1 \cos(2\beta_o z) + n_2 |E(z)|^2 \ , \tag{5}$$

where n_2 is the intensity dependent index of refraction. The intensity dependent index of refraction is related to the third order nonlinear susceptibility by

$$n_2 = \frac{12\pi\chi^{(3)}}{n_o} \ . \tag{6}$$

We will assume that $n_1 << n_o$ and $n_2 << n_o$, and make the slowly varying envelope approximation. Under these conditions the coupled amplitude equations describing the propagation of forward- and backward-propagating waves in the structure can be written as [5]

$$\frac{dA}{dz} = i\kappa B e^{-i2\Delta\beta z} + i\gamma[|A|^2 + 2|B|^2]A \tag{7a}$$

and

$$\frac{dB}{dz} = -i\kappa A e^{i2\Delta\beta z} - i\gamma[2|A|^2 + |B|^2]B \ , \tag{7b}$$

where $\gamma = \pi n_2/\Lambda$ is the nonlinear coupling constant. These equations can be solved to predict the transmission characteristics of the nonlinear distributed feedback structure. At low intensities, light will be transmitted through the periodic structure when the frequency of the light is well outside the stop gap. The light will be reflected when the frequency falls within the stop gap. However, if the index of refraction of the structure is intensity dependent, the expected low intensity behavior can be dramatically modified. For example, consider the transmission of light whose frequency is tuned to the center of the stop gap ($\Delta\beta$=0) of a DFBS with a positive intensity dependent index of refraction. For low intensities the transmission of the structure will be low due to the strong coupling between the forward- and backward-propagating waves. As the intensity is increased the average index will increase and the stop gap will appear to shift to lower frequencies. This change in index will decrease the coupling between the forward- and backward-propagating waves and result in an increase in transmission.

Figures 4 and 5 show a plots of the transmission that were obtained by solving the coupled amplitude equations (7) for the case of a nonlinear DFBS with κL=4.0 and γLE_c=1.0 where the critical intensity is $E_c = 4n_o\lambda/3\pi\gamma\Lambda L$. Figure 4(a) shows the predicted transmission of the DFBS as a function of detuning when the incident intensity is very low (i.e. the nonlinear term in the index is not important). The dependence of the transmitted intensity on incident intensity was then studied for the three detunings marked (I), (II) and (III) in Fig. 4(a). Figure 4(b) shows the dependence for the case of $\Delta\beta L$=4.2. The intensities are normalized to a critical intensity. For this detuning we see that the coupled amplitude equations predict that the structure will switch from a low to high transmission state at specific intensities. Figure 5(a) displays the case when the frequency of the incident light is tuned to the center of the stop gap ($\Delta\beta L$=0). At this detuning we see that the transmission exhibits optical bistability. For certain incident intensities there are three possible values of the transmitted intensity. It has been shown that the dashed region is unstable, so there are only two possible stable values. [13]

When the frequency of the incident light is tuned to the low frequency edge of the stop gap the solution to the coupled amplitude equations show that the transmitted intensity is multistable for a certain range of incident intensities (Fig. 5(b)). On fig. 5(b) the unstable regions are denoted by dashed lines.

Along with the steady state characteristics, the temporal dependence of the transmission has been studied extensively. Under certain conditions, some of the bistable states predicted by the steady-state theory are found to exhibit temporal fluctuations. Numerical calculations have shown that for a field with a frequency tuned the center of the stop gap of a nonlinear DFBS with a large κL, the upper branch of the bistability curve predicted by the steady state theory is unstable and the transmission of the nonlinear DFBS exhibits periodic self pulsing for intensities above the switching intensity [10-12]. If the intensity is increased to many times the switching intensity the temporal fluctuations become chaotic. A linear stability analysis performed by de Sterke [13] confirmed that there are many regions where the high-transmission state predicted by steady-state theory is temporally unstable. He found that as the frequency of the incident field is tuned deeper into the stop gap, the system tends to become more unstable.

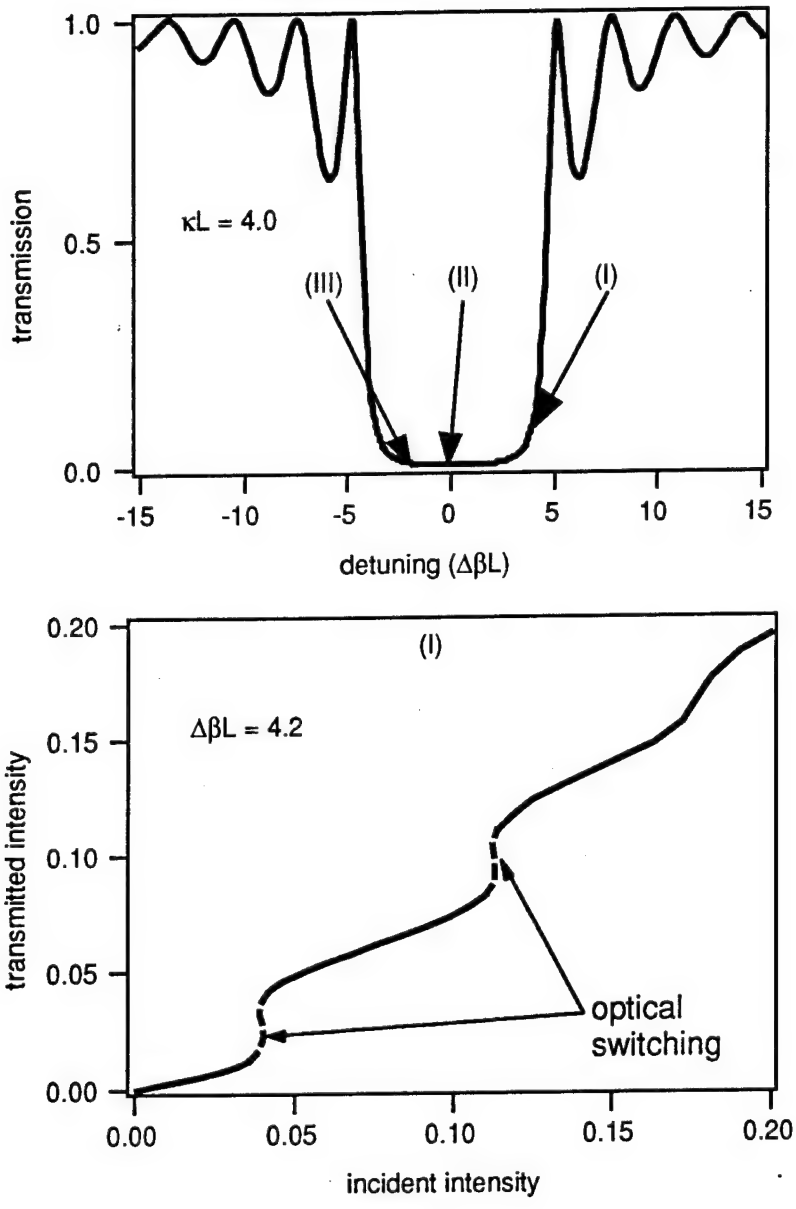

Figure 4. *(a) The transmission of the nonlinear DFBS plotted as a function of detuning for the case of κL=4.0 and very low intensity. (b) The transmitted intensity plotted as a function of incident intensity for a detuning of $\Delta\beta L$=4.2.*

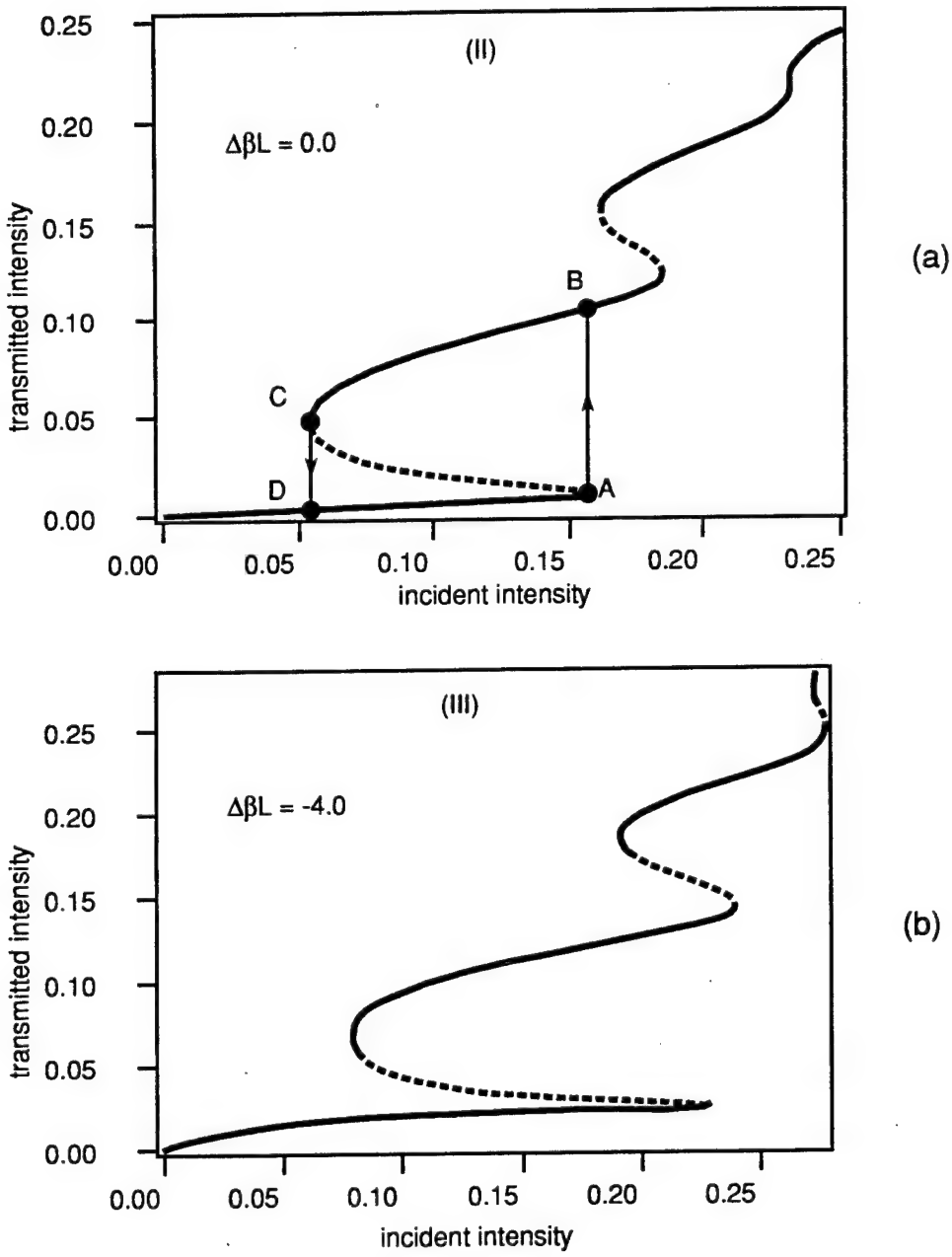

Figure 5. *The transmitted intensity plotted as a function of incident intensity for (a)*$\Delta\beta L=0.0$ *and (b)* $\Delta\beta L=-4.0$.

Soliton formation in nonlinear DFBS have also been studied theoretically. When the frequency of the incident field is tuned outside the stop gap, soliton formation is possible due to the dispersion of the periodic structure and the nonlinearity of the media. These solitons display characteristics that are similar to those supported in nonlinear optical fibers. In this limit the nonlinear periodic structure is predicted to be useful for pulse compression [14]. When the frequency of the incident light is tuned within the stop gap, soliton formation is also predicted and in this case the soliton is often referred to as a gap soliton [15-19]. A gap soliton is excited under conditions when the transmission is predicted to be bistable. A striking characteristic of gap solitons is that they can propagate through the nonlinear DFBS with velocities that are much lower than the group velocity of light in such a medium.

II. Nonlinear Optical Properties of Colloidal Crystals

Several material systems have been proposed for use as nonlinear DFBS. Many of the proposed systems utilize waveguide structures such as optical fibers or planar waveguides. A desired property of these structures is that high intensities can be propagate over large distances. The system of a corrugated silicon-on-insulator waveguide has been studied experimentally be Snakey et al [23,24]. However in many of these systems other nonlinear effects must be considered such as nonlinear coupling effects. In our work we have chosen to use a bulk geometry since the nonlinearity of the system is large enough to allow a short sample length. The material we have used in this study is a colloidal crystal comprised of polystyrene spheres dispersed in water [1-3]. The lattice spacing of the colloidal crystal is comparable to the wavelength of light. The index of refraction of the polystyrene is 1.59 and the index of refraction for water at room temperature is 1.33. The alternating crystal planes create a periodic index of refraction which is utilized as the nonlinear DFBS.

II.A. Colloidal Crystals

A colloidal crystal is a monodispersed suspension of uniformly charged polymer spheres in water, which forms a periodic array due to a screened Coulombic force between each sphere [25,26]. The polymer spheres used in our experiments were composed of polystyrene with negatively charged ionic sulfunate groups attached to the surface of the spheres. The lattice spacing between

the array planes is typically between 0.1 to 10 μm. There are three phases that can be formed by the colloidal suspension: a face centered cubic (FCC), a body centered cubic (BCC), or an amorphous structure. The filling fraction, electric charge per sphere, number of ions in solution, and temperature of the suspension are all important parameters in determining the array structure of the colloidal suspension. The filling fraction ϕ_v is the fraction of the total volume occupied by the polymer spheres. For high filling fractions and low ion concentrations, such as used in our experiment, the suspensions usually form a FCC structure, which is shown schematically in Fig. 6.

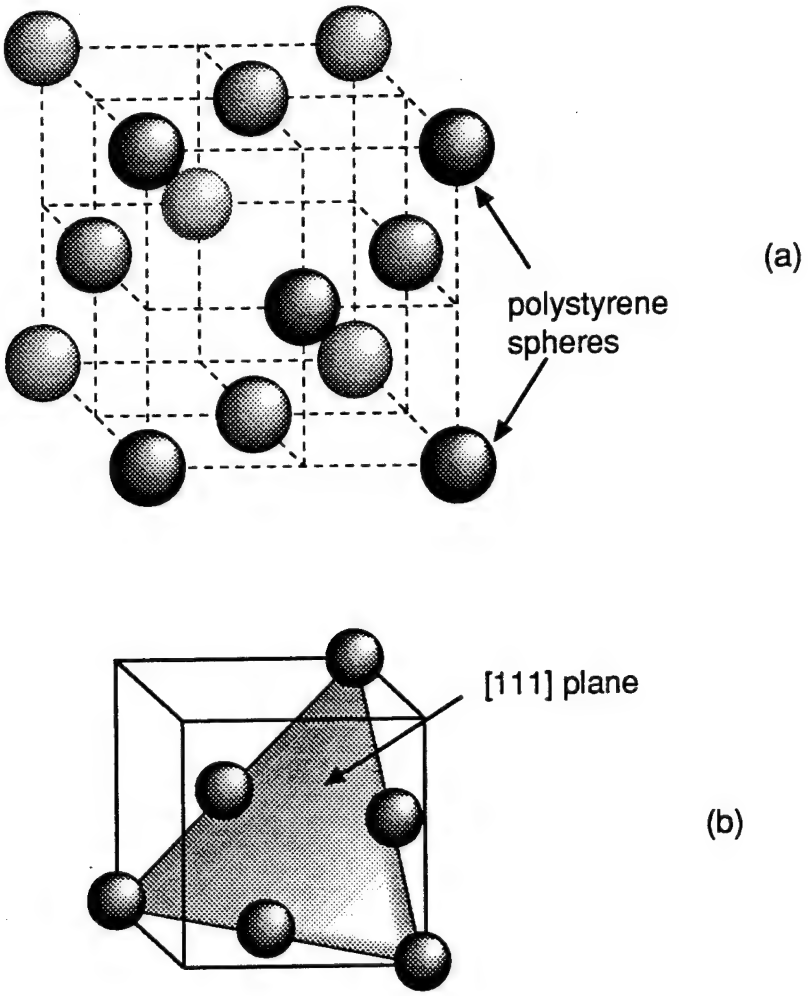

Figure 6. *(a) A schematic representation of a unit cell of a colloidal crystal in the FCC phase. (b) Some spheres have been removed in the figure to show a [111] plane bisecting a unit cell. Only the spheres that comprise this plane are shown.*

For our experiments, monodispersed latex suspensions of 120 nm polystyrene spheres with charged sulfonate groups on the surface of the sphere were obtained from the Emulsions Polymer Institute at Lehigh University. These solutions were diluted with distilled water until they appeared to be iridescent orange in color. The color is due to Bragg scattering of the incident light off the [111] plane of the array whose structure is FCC. The color of the reflected light indicates the wavelength of the Bragg resonance. By adding the appropriate amount of water, we can tune the lattice spacing of the array and thereby tune the center of the stop gap. When preparing the sample, we start with a small fraction of the latex suspension that was placed in a test tube and decrystallized using an extremely dilute solution of HCl. The ions from the HCl screen the individual charges of each sphere reducing the repulsive force between spheres. Care must be taken to prevent flocculation during this procedure. The solution was then placed in a cuvette with a thickness of 100 μm and deionizing resin was placed at one end of the cuvette. The cuvette was then sealed using paraffin wax to prevent evaporation. As ions are removed by the resin, the repulsive force between each sphere increases and the array forms. Crystal growth begins at the edge of the solution in contact with the resin and grows outward until most of the length of the container is filled. The colloidal crystals typically grow with the [111] plane of the array parallel to the wall of the cuvette.

The colloidal crystals are characterized by observing Kossel rings formed by the scattered light [27] and measuring the transmission of the crystal as a function of wavelength. Figure 7 shows the transmission spectrum for a 100 μm thick colloidal crystal made from a solution of 120 nm diameter polystyrene spheres. Also shown in the figure is a theoretical fit to the experimental data that was obtained by solving the coupled amplitude equations. The coupling constant used for this fit was $\kappa L=3.5$.

II.B. Nonlinear Optical Properties of Colloidal Crystals

The nonlinear optical properties of the colloidal crystals were studied using a nonlinear interferometer [28]. We conclude from this measurement that electrostriction is the dominant intensity dependent effect in these suspensions and we believe it to be responsible for the nonlinear phenomena observed such as optical limiting and optical bistability. Electrostriction is the tendency for material with a higher dielectric constant to be pulled into regions of space with

large electric fields. In the experiment an interferometer was used to measure the phase change of a probe beam that was induced by the presence of an intense pump beam. To eliminate the effects of the index grating of the periodic structure, the frequencies of both the probe beam and the pump beam were chosen to be far from Bragg resonance.

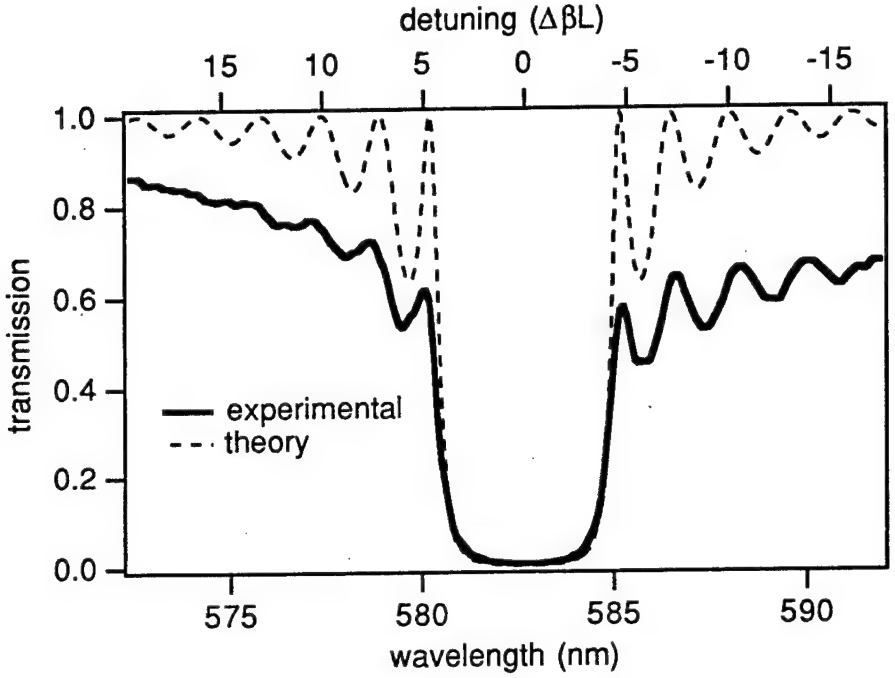

Figure 7. *The transmission spectrum of a colloidal crystal comprised of 120 nm polystyrene spheres is represented by the solid line. A fit using the coupled amplitude equations is plotted as the dashed line.*

Figure 8 shows a schematic diagram of the interferometer used to measure the nonlinear index of refraction of the colloidal crystal. The measurement entailed comparing the interference pattern at low intensity, where the nonlinear response is assumed to be small, to an interference pattern recorded in the presence of the strong pump beam.

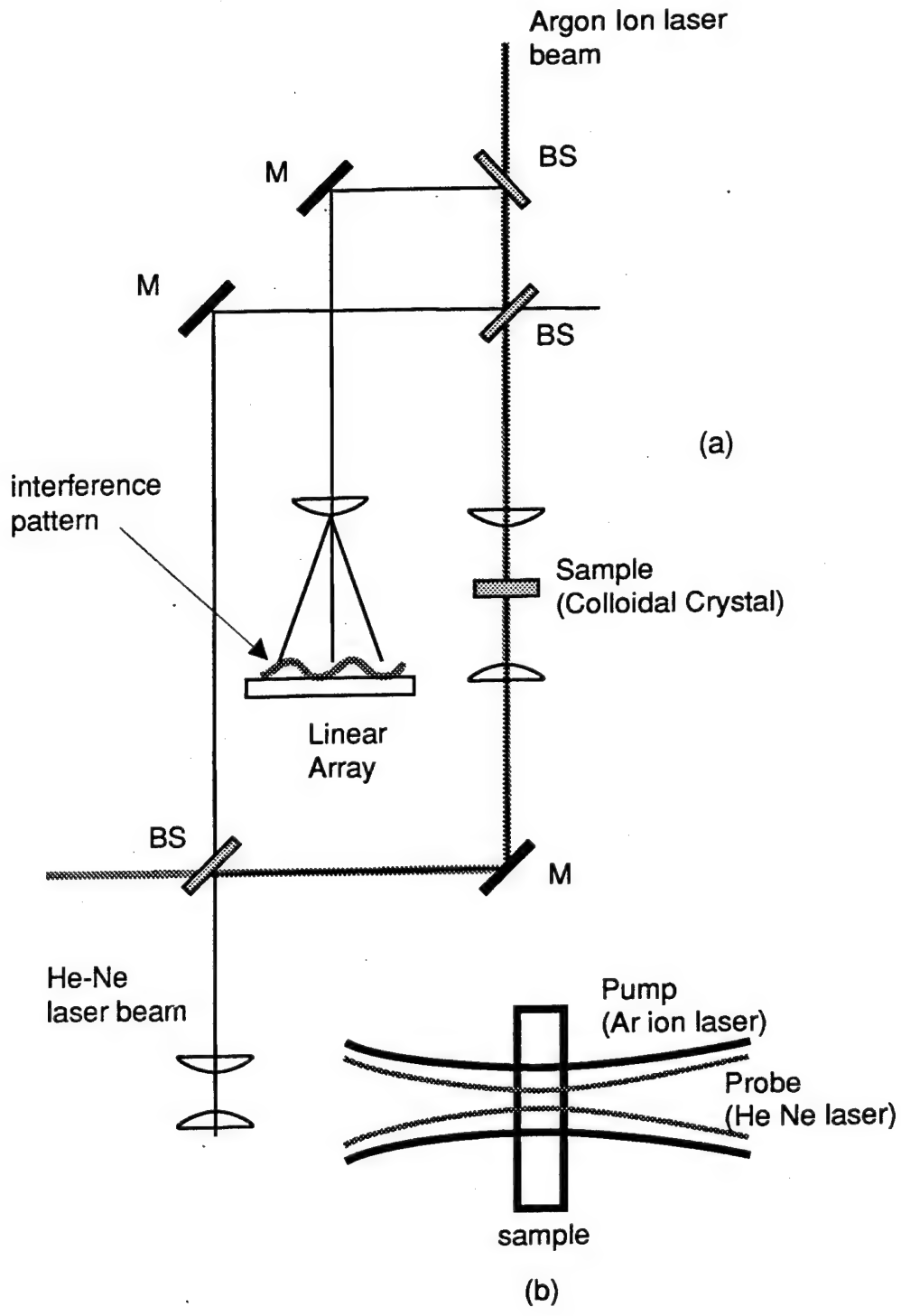

Figure 8. *Schematic diagram of the nonlinear interferometer.*

Consider coherent light from the probe laser that enters the dielectric medium with an initial phase ϕ_o. The phase of the wave after passing through the medium is

$$\phi = \frac{2\pi Ln}{\lambda_{vac}} + \phi_o \tag{8}$$

where L is the length of the sample, n is index of refraction of the medium and λ_{vac} is the vacuum wavelength of the probe light. We assume the index of refraction of the medium has an intensity dependent contribution and can be written as $n = n_o + n_2 I$. The phase can now be separated into a linear and nonlinear contribution, $\phi = \phi_{linear} + \Delta\phi$, where ϕ_{linear} is the phase at low intensities and $\Delta\phi$ is the change in phase due to the nonlinear index of refraction. Using these expressions we can write an expression for the nonlinear index of refraction in terms of the induced phase shift

$$n_2 = \frac{\Delta\phi\lambda_{vac}}{2\pi LI} . \tag{9}$$

Any change in index of the sample will change the phase of the light in one arm of the interferometer and therefore shift the resulting interference pattern.

Two separate lasers where used as pump and probe in this experiment. An argon ion laser was used to modify the index of refraction and is referred to as the pump laser. The second laser, called the probe laser, was a low power helium-neon laser and was used in the interferometer to monitor the change in index. The pump laser only passes though the sample and not the interferometer. The pump beam was focused onto the sample to a spot size of approximately 10 μm. The probe beam was counterpropagating with respect to the pump beam and had a slightly smaller radius of 7 μm. The interference pattern produced by the interferometer was monitored using a photodiode array. The interferogram was recorded with the pump beam off as a reference pattern. The pump beam was then turned on and aligned to maximize the fringe shift.

The experimental results that were obtained using a 500 μm thick sample are shown in Fig. 9. The solid line represents the interference pattern obtained with the pump beam blocked, while the

dashed line represents the pattern obtained with a pump beam intensity of 1 MW/cm^2. From the fringe shift we have estimated the change in index to be $\Delta n = 5 \times 10^{-4}$, which suggests that the volume fraction increased by $\Delta\phi_v \approx 0.0025$. In addition to the magnitude of the index change, the sign of the index change was obtained by noting the direction of the fringe shift and comparing it against a known nonlinearity. We noted that the direction of the fringe shift was opposite to the direction when an absorptive dye was used as the sample. In the case of the absorptive dye the nonlinearity was thermal and therefore the index change was negative. From our measurements we estimate that the intensity dependent index of the colloidal crystal is $n_2 = 5 \times 10^{-10}\ cm^2/W$.

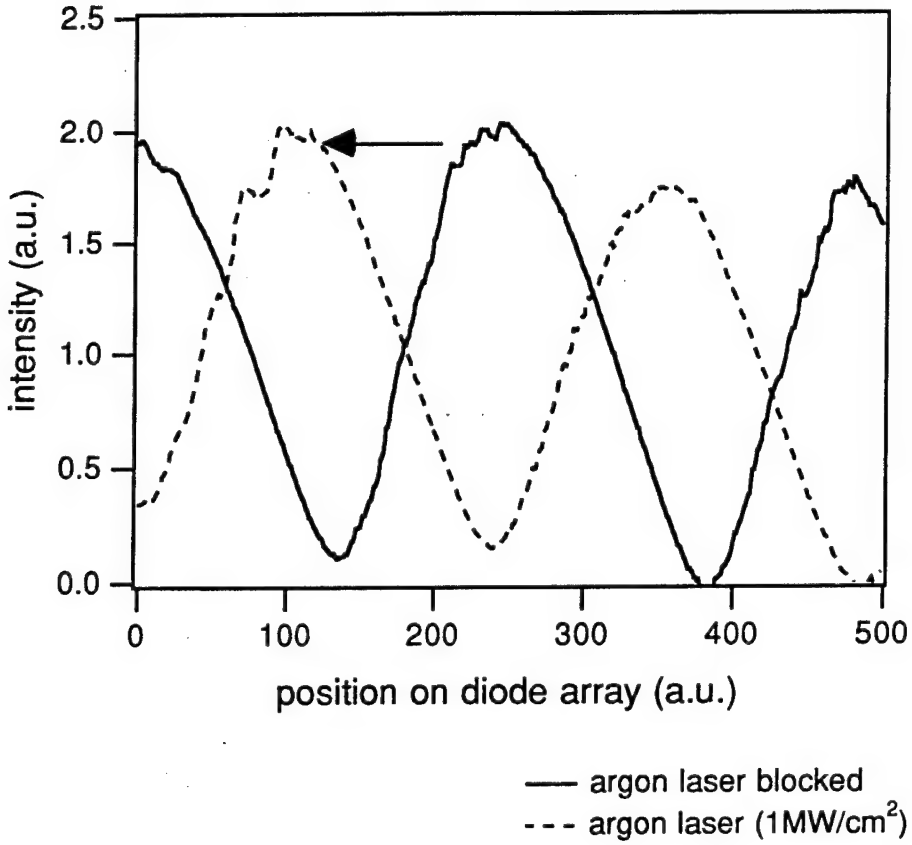

Figure 9. *The interference pattern produced by the nonlinear interferometer. The solid line represents the interference pattern obtained with the pump beam blocked. The dashed line represents the interference pattern obtained when the pump beam was unblocked.*

With the interferometer measurement we feel that the positive intensity dependent index indicates that the nonlinearity is not a thermal nonlinearity. We believe that the source of the nonlinear change in the index of refraction is electrostriction.

For a nonlinear DFBS with a fixed index grating and a positive intensity dependent index of refraction we expect to observe simple switching on the high frequency edge of the stop gap, and bistability and multistability for frequencies near the low frequency edge of the stop gap. As will be discussed in the next section we see the opposite for the case of the nonlinear colloidal crystals. We believe that we obtain these results because in the case of the colloidal crystals the array planes are not rigidly fixed in space. For the case when the frequency of the light is tuned near Bragg resonance there can be an electrostrictive force that compresses the lattice in the direction that light propagates. When the lattice compresses the average index of the DFBS increases as the concentration of the polystyrene spheres increases as was seen in the interferometer measurement. This increase in index will lead to a shift of the Bragg wavelength to longer wavelengths. However, the compression will also lead to a decrease in the lattice spacing which will decrease the Bragg wavelength. Of these two effects, we estimate that the decrease in the lattice spacing leads to the largest shift in Bragg resonance.

Near Bragg resonance we expect that the largest electrostrictive effect results from the spatially varying electric field inside the DFBS [29]. This contribution is expected to be much larger than the electrostriction resulting from either the radial field gradient produced by the Gaussian nature of the laser beam or the field gradient resulting from the slowly varying field amplitude along the length of the structure. For the case of two counterpropagating beams in a colloidal crystal, the field gradient resulting from the spatially varying field was calculated to be two orders of magnitude larger than the radial gradient for a spot size of ~10 μm [30]. The theoretical study by Russell [29] showed that the field inside a periodic structure oscillates in space on the order of one grating period when the frequency of the field is near Bragg resonance. The maxima of the oscillations overlap with the high-index layer of the periodic structure when the frequency of the incident light is tuned to the low-frequency edge of the stop gap. For this detuning the

electrostrictive force will be a minimum. As the frequency of the light is increased toward the high-frequency edge of the stop gap the intensity maxima move away from the high index layer until at the high-frequency edge the minima overlap the high-index layers. The electrostrictive force will therefore be intensity and frequency dependent, and will increase as the detuning from the low-frequency edge of the stop gap is increased.

II.C. Optical Power Limiting

An optical power limiter is a device with a constant transmission at low intensities and an ever decreasing transmission at high intensity. Ideally, an optical limiter prevents the transmitted intensity from exceeding a prescribed intensity. An optical limiter may therefore be used to protect sensitive equipment such as a photodetector from large fluctuations in intensity that may cause optical damage. Optical power limiting has been observed in several optical systems that employ an intensity dependent index of refraction. The majority of these systems use the self defocusing effect in combination with an aperture. The size of the beam inside the limiter is intensity dependent and therefore the transmission through the aperture intensity dependent [31,32].

Nonlinear DFBS have been predicted to exhibit power limiting for frequencies near the edge of the stop gap [4]. For a colloidal crystal the largest change in transmission will result from the change in lattice spacing when the crystal is illuminated by high intensity light whose frequency is tuned near the stop gap. The experimental setup used to measure the transmission of the colloidal crystal is illustrated in Fig. 10. An argon ion laser operating on the 514 nm lasing transition was used as the high intensity light source. Since the source was not tunable, the lattice spacing of the crystal was chosen so that the high frequency edge of the stop gap coincided with the frequency of the laser. A beam chopper with an on and off time of ~100 μs was used so that the response time of the limiter could be measured. Following the chopper, a beam sampler was placed in the laser beam to monitor the incident light. The laser beam was then focused to a spot size of ~45 μm at the sample. The sample was placed at the center of the confocal region of the focused beam. The transmitted light was then focused onto a detector.

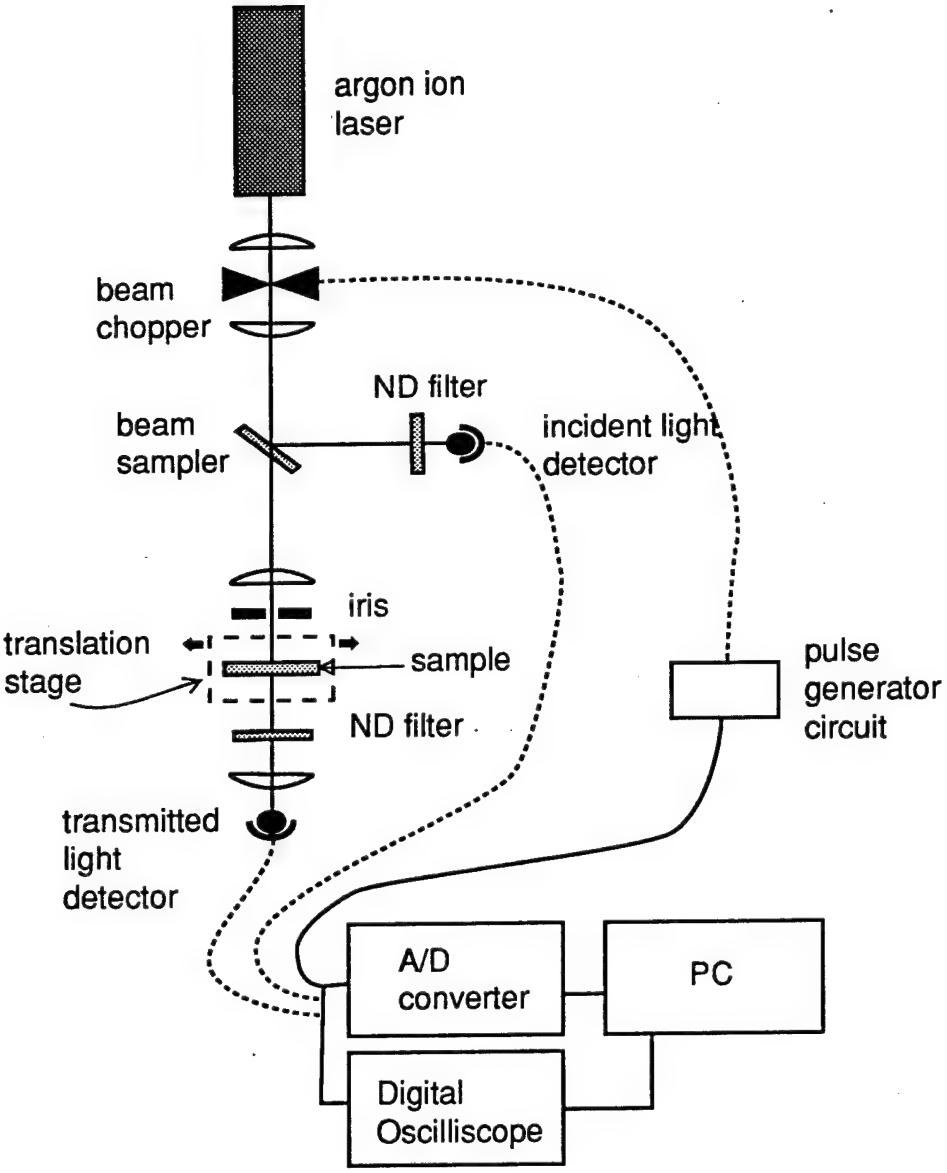

Figure 10. *The experimental setup used to characterize the optical limiting.*

For these experiments, the sample used consisted of a suspension of 86 μm diameter polystyrene spheres contained in a 100 μm thick cuvette. The Bragg wavelength was estimated by measuring the angular size of the Kossel ring. For the samples used in this experiment, the angular size for an illumination wavelength of 514 nm was measured to be ~6° which means that the center of the stop gap was at ~510 nm.

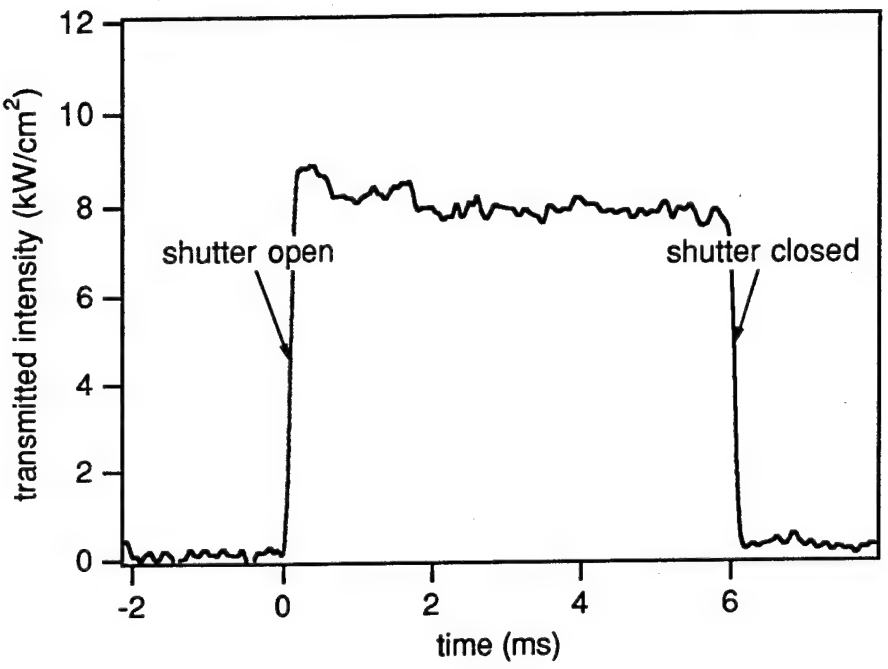

Figure 11. *Transient behavior of the transmitted intensity for an incident intensity of 100 kW/cm^2.*

To measure the response time of the optical limiting, the signals from the photodetectors were recorded as a function of time using a digital oscilloscope. The light from the laser was chopped such that a pulse with a duration of 6 ms would pass through the crystal approximately once per second. Fig. 11 shows the transmitted intensity plotted as a function of time for an incident intensity of 100 kW/cm^2. Although there is a very slight decrease in transmission after the shutter is first opened, the transmission is fairly constant with time. At this intensity the nonlinear effects are small. Fig. 12 shows the transient behavior of the transmitted intensity for higher intensities. The transmission through the sample is high initially and drops to a lower steady state value.

When the shutter first opens the transmission through the sample is nearly the same as the transmission at low intensity. As the sample responds to the field, the transmission drops until the system reaches an equilibrium. The response time was measured to in the range 100 μs to 350 μs.

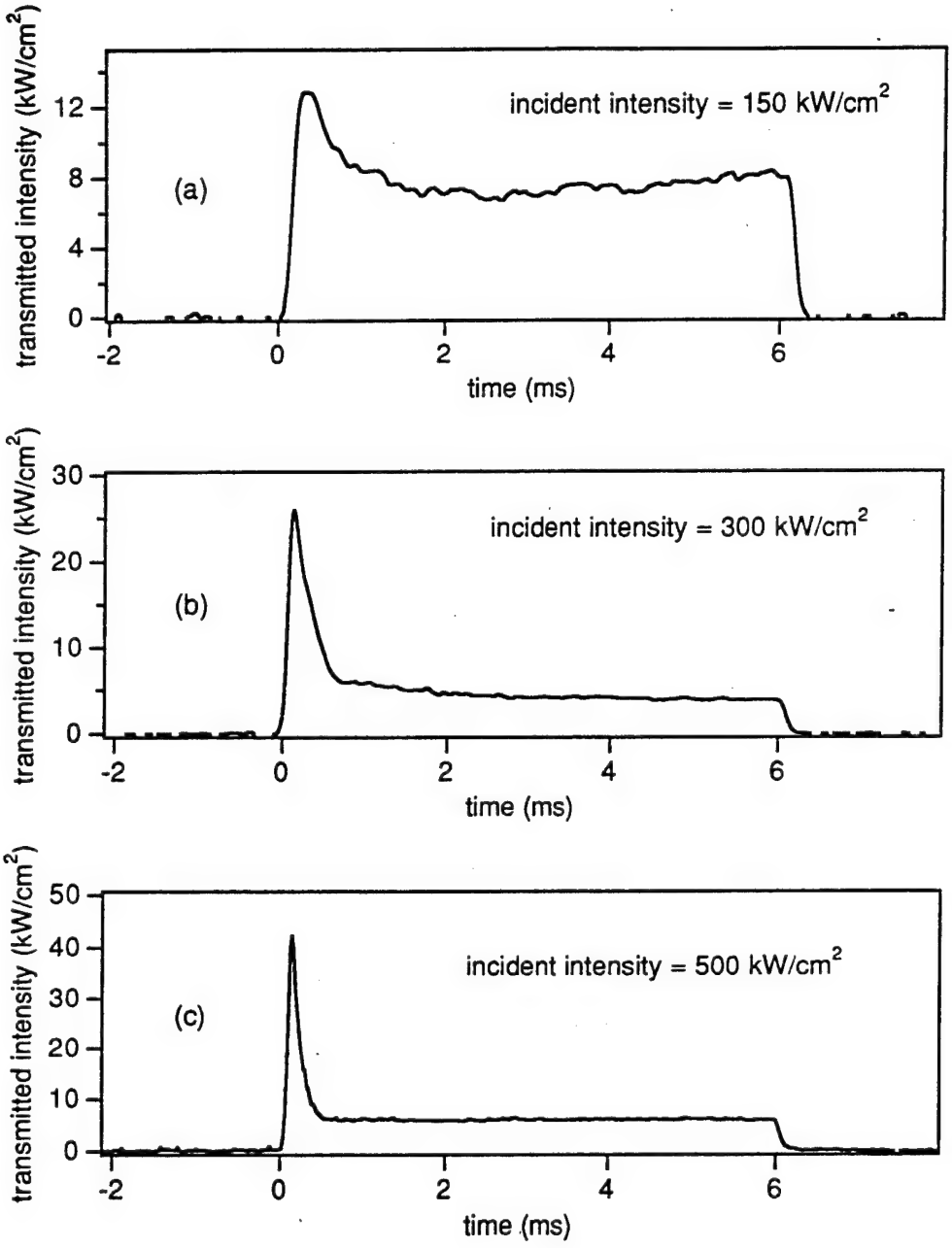

Figure 12. *The transient behavior of the transmitted intensity for incident intensities of (a) 150 kW/cm², (b) 300 kW/cm², and (c) 500 kW/cm².*

To characterize the optical limiting we measured the steady state transmission of the colloidal crystal as a function of incident intensity. Preliminary transmission measurements showed that the samples experienced damage when exposed to intense light ($I > 100$ kW/cm^2) for approximately a second or longer. We therefore limited the illumination time to several milliseconds so that the time average intensity remained low. The transmission measurements were taken after the system reached steady state.

Figure 13 shows a plot of the transmitted intensity versus incident intensity for a frequency that is tuned to the high frequency side of the stop gap (λ=514 nm). From this data we can see that the transmission of the colloidal crystal decreases at high intensities. At low intensities the transmission of the sample was measured to be nearly 30%. As the incident intensity was increased, the transmission remained roughly constant up to an incident intensity of ~80 kW/cm^2. At higher intensity the transmission drops rapidly. The limiting intensity for the sample was approximately 15 kW/cm^2.

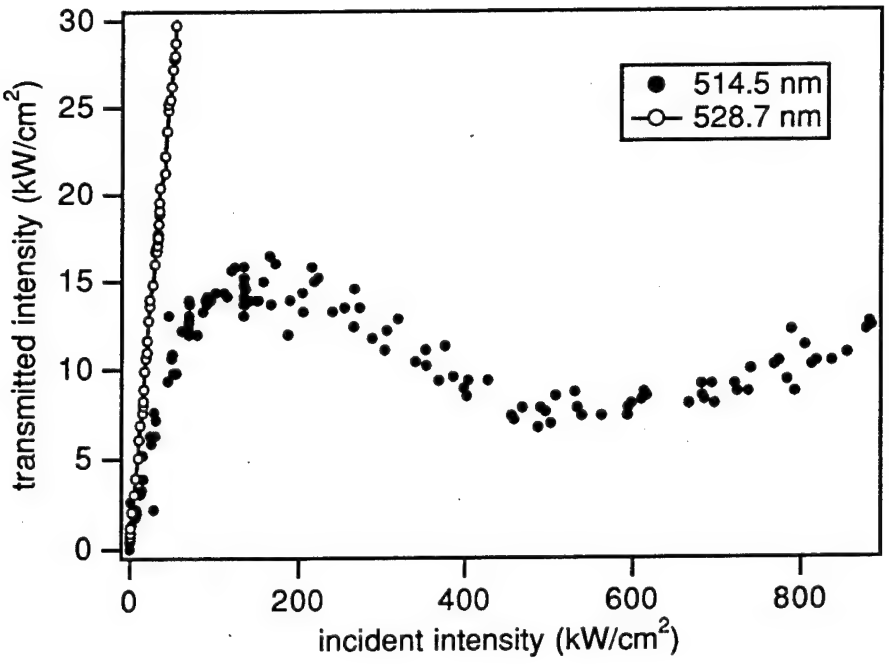

Figure 13. *The transmission of the colloidal crystal is shown for wavelengths of 514 nm (solid circle) and 528 nm (open circle).*

II.D. Optical Switching and Bistability

To study the switching properties of the colloidal crystals we have measured the transmission for the case when the frequency of the laser is tuned with in the stop gap. In this case we find optical switching, optical bistability and multistability.

The experimental apparatus used to study optical switching and optical bistability is shown schematically in Fig. 14. The dye laser was operated with Rhodamine 6G to provide a tunable source in the wavelength range 560 nm to 610 nm. The laser beam was focused through the sample with a 63 mm focal length lens. The spot size at the sample was measured to be 10 μm and the confocal parameter of the laser beam was 8 mm, which was much longer than the cell length of 100 μm. The light transmitted through the sample was focused onto a calibrated detector located directly behind the sample holder.

The measured transmission is plotted as a function of wavelength in Fig. 15 as the solid line. This data was taken at low intensity (50 W/cm^2) while the laser wavelength was scanned from approximately 570 nm to 595 nm. A calculated plot of the transmission of a periodic structure with a coupling constant κL=3.5 is shown in Fig. 15 as the dashed line. The theoretical plot was fit to the experimental data by adjusting the Bragg wavelength and the coupling constant in the coupled amplitude equations. The value of L was held fixed at 100 μm. The letters and arrows indicate wavelengths at which the data plotted in Figs. 16 - 19 were recorded.

When the laser was tuned to a wavelength of 583.0 nm, labeled (A) in Fig. 15, the transmission of the sample was found to be nonlinear and showed a gradual increase in transmission as a function of increasing intensity. Fig. 16(a) shows the transmitted intensity plotted as a function of incident intensity at this detuning. When the laser is tuned deeper into the stop gap a more rapid increase in transmission is observed as shown in Fig. 16(b). The wavelength of the laser for this case was 582.5, which is denoted by point (B) in Fig. 15.

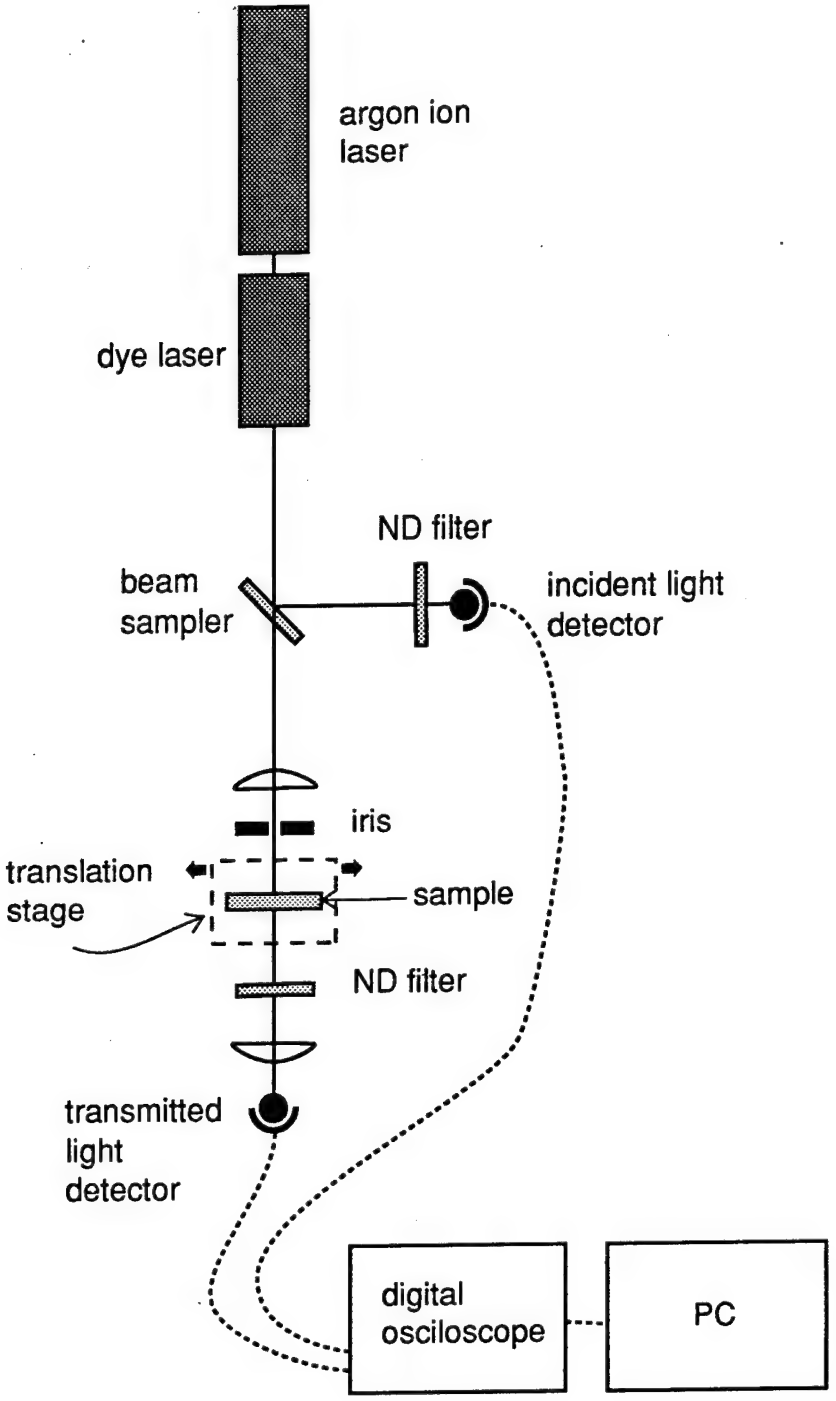

Figure 14. *The experimental setup used to observe optical switching and bistability.*

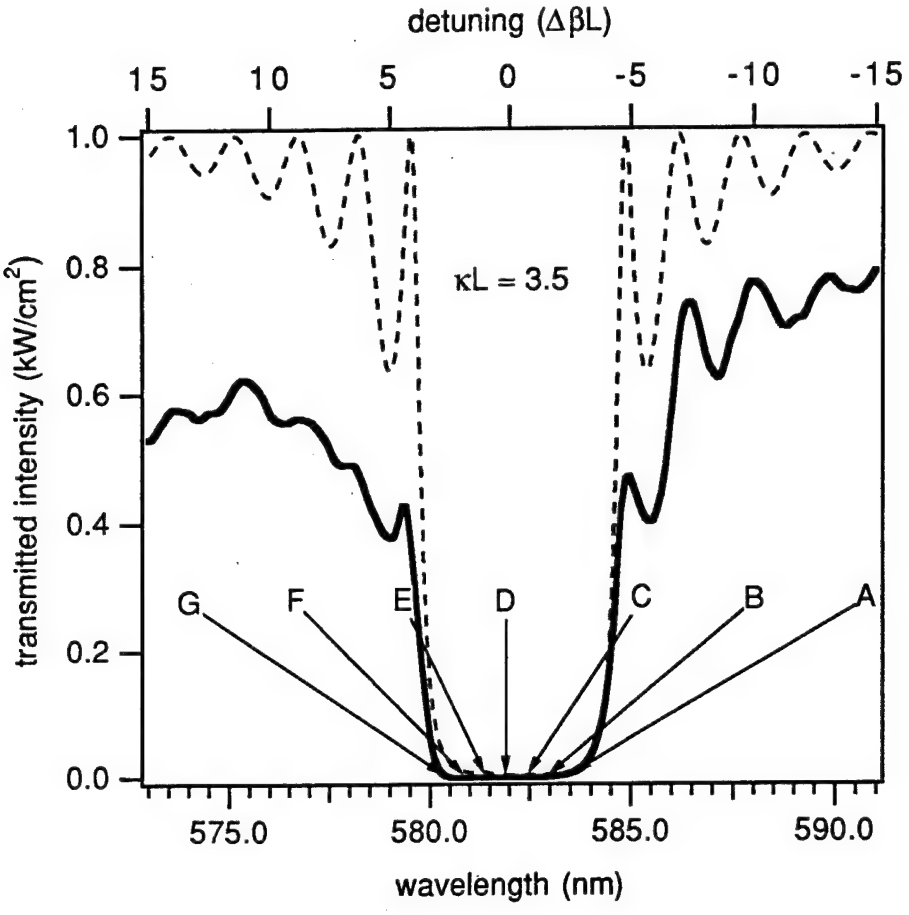

Figure 15. *The transmission of a 100 μm sample is plotted as a function of wavelength. The letters indicate different detunings at which the data plotted in Figs. 16-19 were recorded The theoretical fit to the experimental spectrum is shown by the dashed line.*

For a wavelength of 582.0 nm (point (C) in Fig. 15) The transmission of the sample shows a discontinuous increase at a critical intensity. Fig. 17(a) shows the transmitted intensity plotted as a function of incident intensity for this case. The switching intensity is approximately 75 kW/cm^2. When the laser was tuned to 581.7 nm the transmission was bistable, which is shown in Fig 17(b). This case is denoted by point (D) on Fig. 15. We found that both the high transmission branch and low transmission branch were stable over time periods exceeding several minutes.

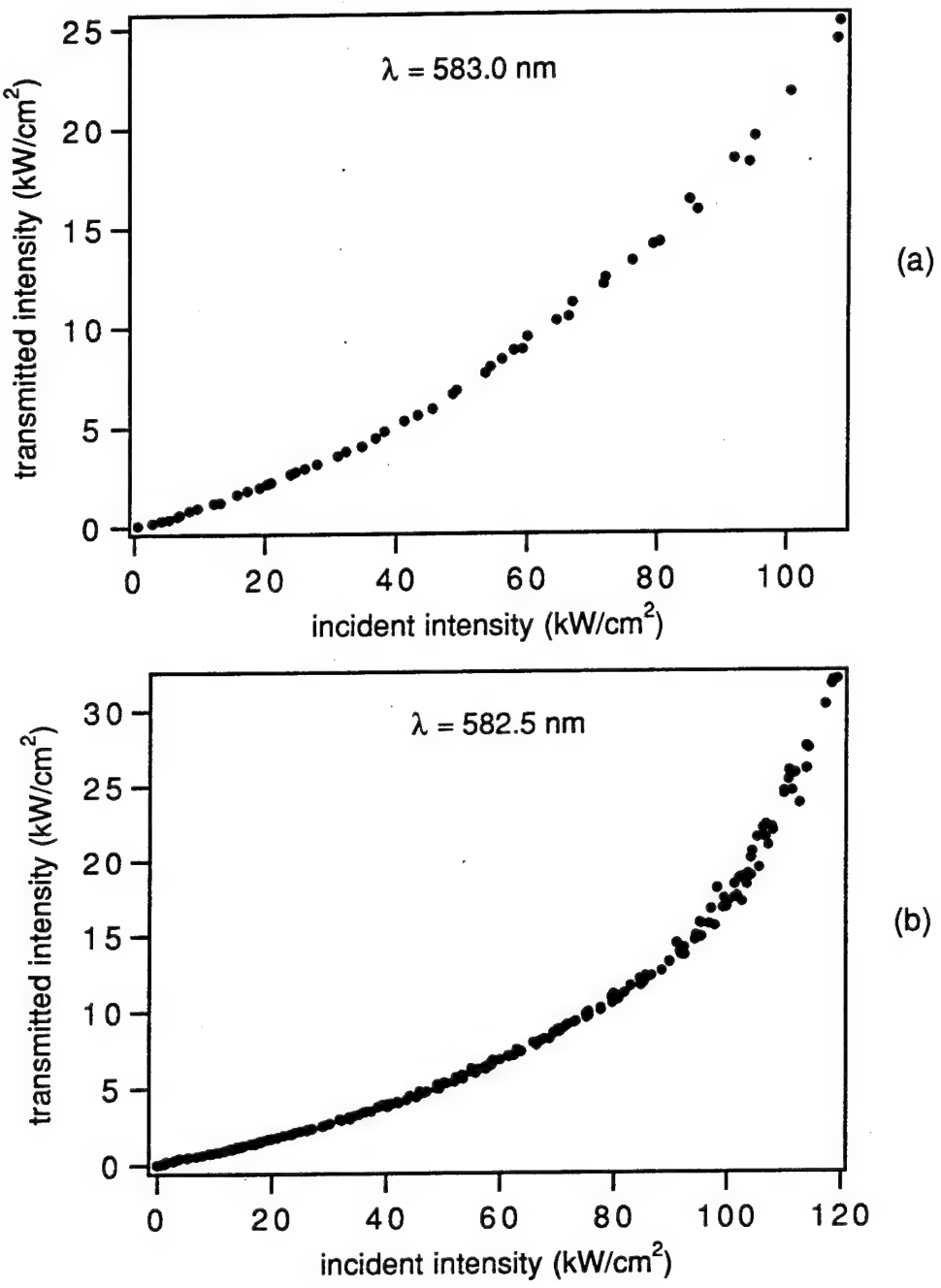

Figure 16. *The dependence of the transmitted intensity on the incident intensity is shown for the case when the laser is tuned to (a) 583.0 nm and (b) 582.5 nm.*

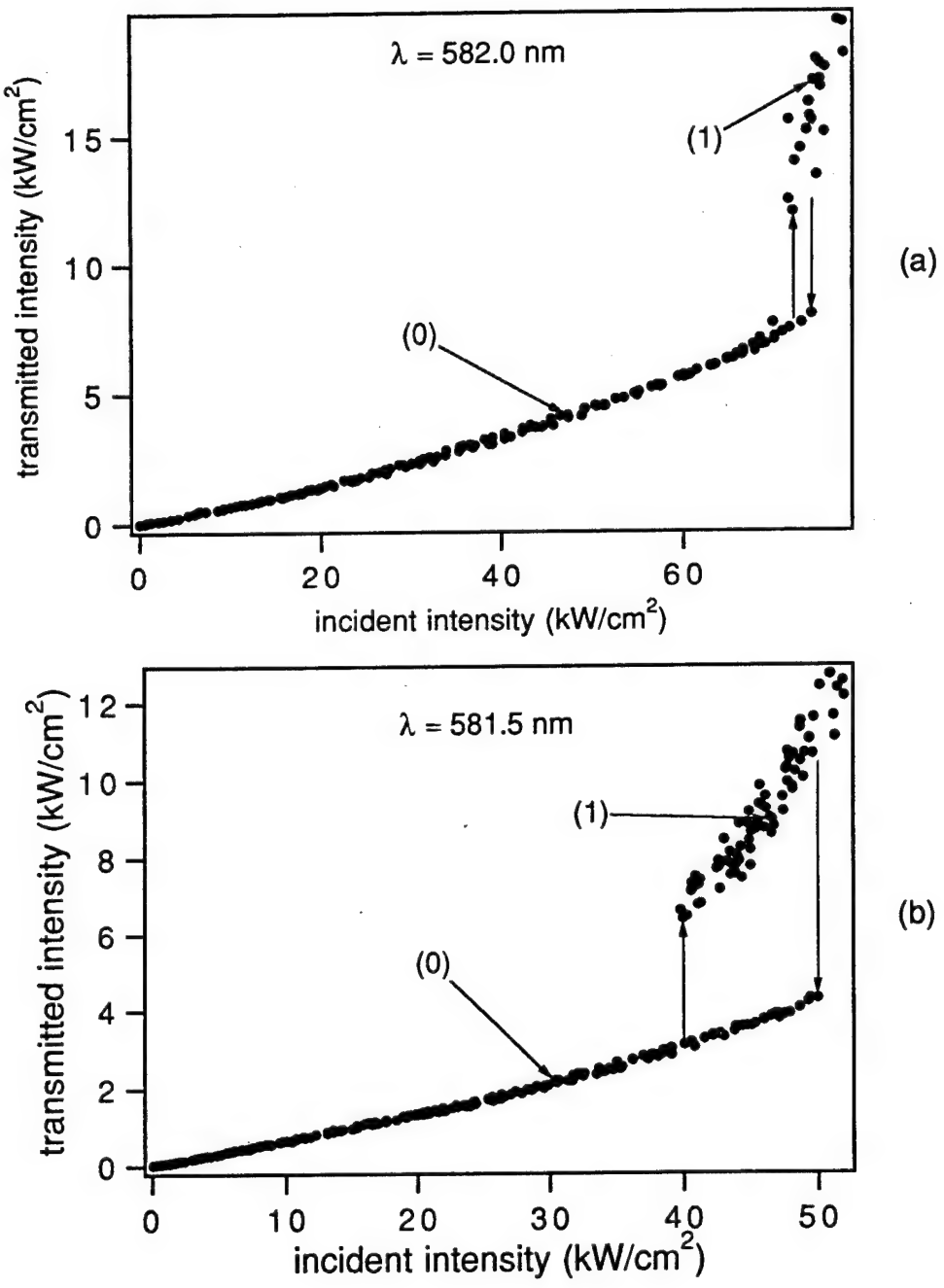

Figure 17. *The dependence of the transmitted intensity on the incident intensity is shown for the case when the laser is tuned to (a) 582.0 nm and (b) 581.5 nm.*

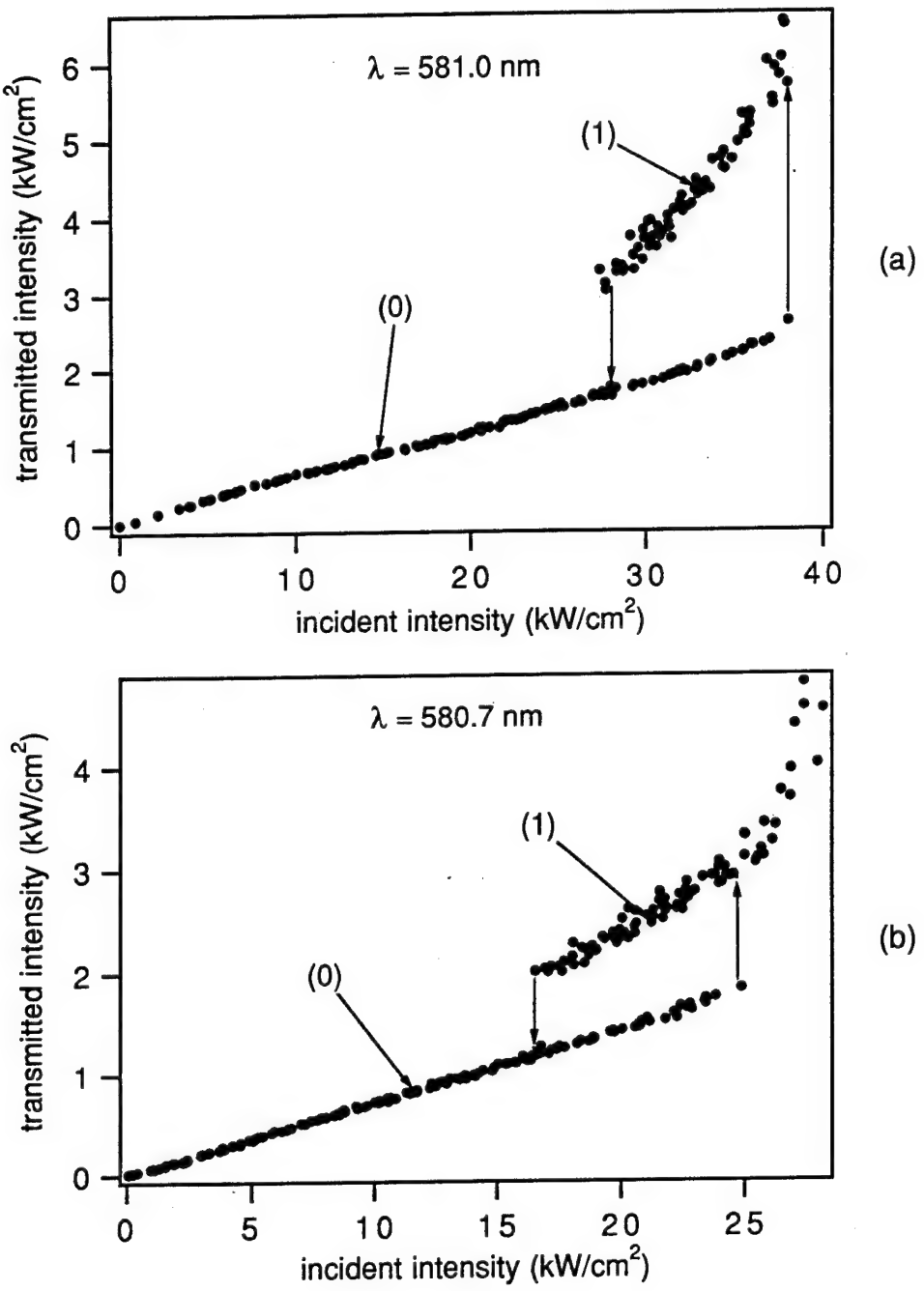

Figure 18. *The dependence of the transmitted intensity on the incident intensity is shown for the case when the laser is tuned to (a) 581.0 nm and (b) 580.7 nm.*

As the laser was tuned to even shorter wavelengths the transmission was also bistable. However as the wavelength was tuned deeper into the stop gap the switching threshold was observed to decreased. Fig. 18(a) and (b) shows the transmission plots recorded at wavelengths of 581.0 nm and 580.7 nm respectively (points (E) and (F) on Fig. 15). When the wavelength was tuned even deeper into the stop gap the transmission was observed to be multistable, as can be seen in Fig 19(a). Fig 19(a) was recorded at a wavelength of 580.5 nm.

For even shorter wavelengths the transmission of the system was unstable with respect to time. The case of the wavelength of 580.2 nm (point (G) on Fig. 15) is shown in Fig 19(b). At intensities greater than 4 kW/cm^2 the transmission would rapidly switch between high and low values and only an average value is plotted on the figure.

The switching characteristics observed using the colloidal crystal are similar to those predicted by the coupled amplitude equations as can be seen in Figs. 4 and 5. One trend that can be seen in Figs. 4 and 5 is that as the frequency is tuned deeper into the stop gap the switching intensity is expected to increase. However in our experiment we observe that the switching intensity decreases as the frequency of the laser is tuned deeper into the stop gap. We believe that the detuning dependence of the electrostrictive effect discussed above, which results from the rapidly varying field inside the DFBS, may help explain the decrease in the switching intensity. However more theoretical and experimental work is needed to verify this conclusion.

We have also studied the spatial intensity distribution in the far field for the transmitted light and found that as the intensity was increased these patterns changed significantly. The spatial distribution of the transmitted beam was found to be dependent on the transmission state of the colloidal crystal. The patterns became more complex when the transmission of the sample was switched to a second or third upper branch. The experimental setup used to study the spatial distributions was essentially the same as shown in Fig. 14 except that the lens and detector following the sample were replaced by a viewing screen located ~2 m behind the sample.

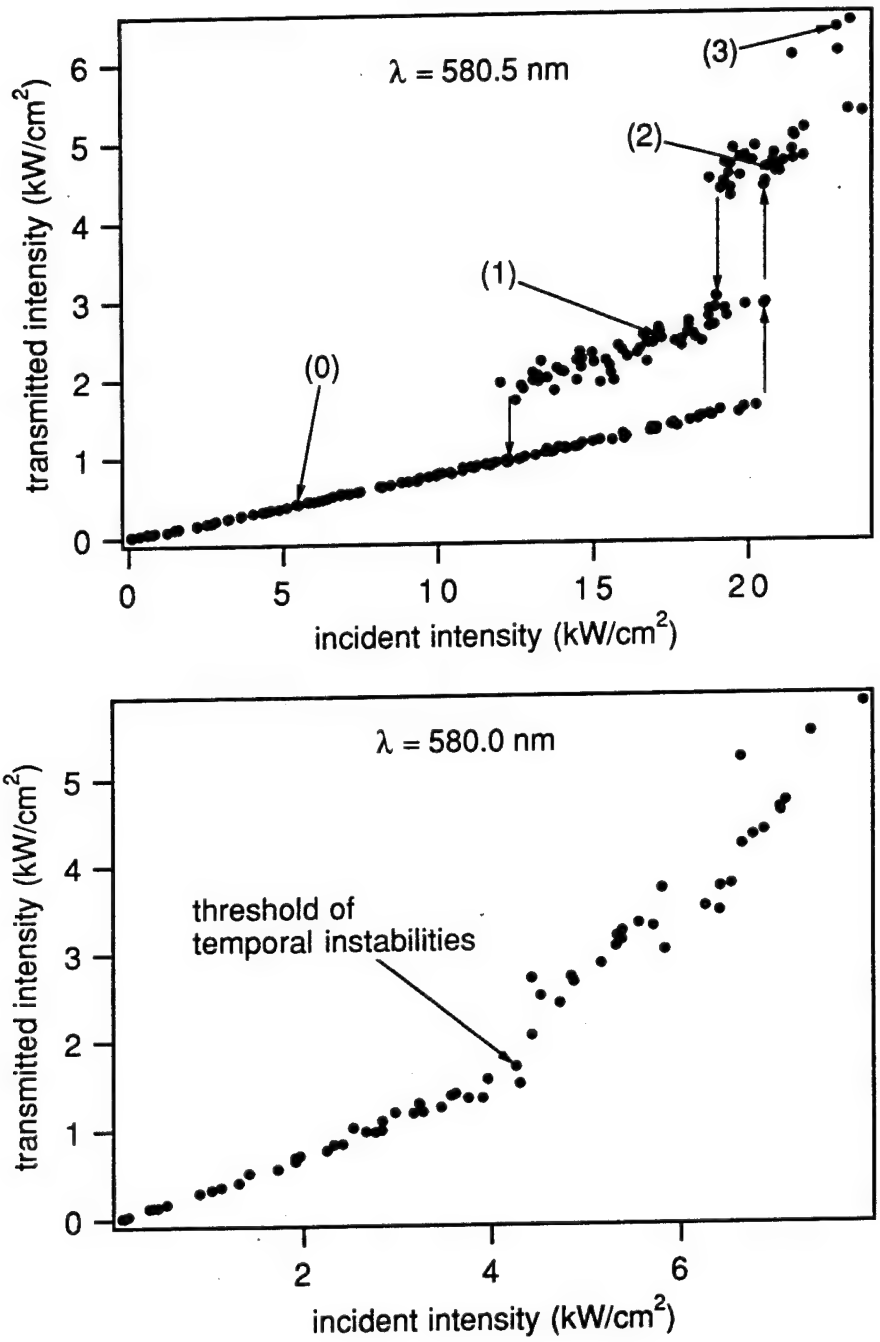

Figure 19. *The dependence of the transmitted intensity on the incident intensity is shown for the case when the laser is tuned to (a) 580.5 nm and (b) 580.0 nm.*

To study the spatial distribution of the intensity the wavelength of the dye laser was tuned near the high frequency edge of the stop gap, which is where the multistable behavior was observed. At low intensities the laser is strongly attenuated while passing through the sample. At this detuning there is very little change in the spatial distribution and the transmitted beam has a gaussian profile. Figure 20(a) shows the transmitted light at low intensity. In addition to the strongly attenuated transmitted beam the Kossel ring which is formed in the scattered light is also visible.

When the intensity is increased and the transmission switches to a high state, the spatial distribution of the transmitted light changes abruptly. Figure 20(b) shows the far field intensity distribution when the transmission has switched to the first upper branch. The beam has expanded and is slightly asymmetric. At even higher intensities the spatial pattern is more complex. Figure 21(a) shows the case when the transmission has switched to the second upper branch. This pattern is very asymmetric and was found to depend on crystal orientation but not on the laser polarization direction. The higher transmitting branches were temporally unstable which made it difficult to record the spatial distribution of the transmitted light. Figure 21(b) shows a pattern obtained slightly below the threshold for oscillation.

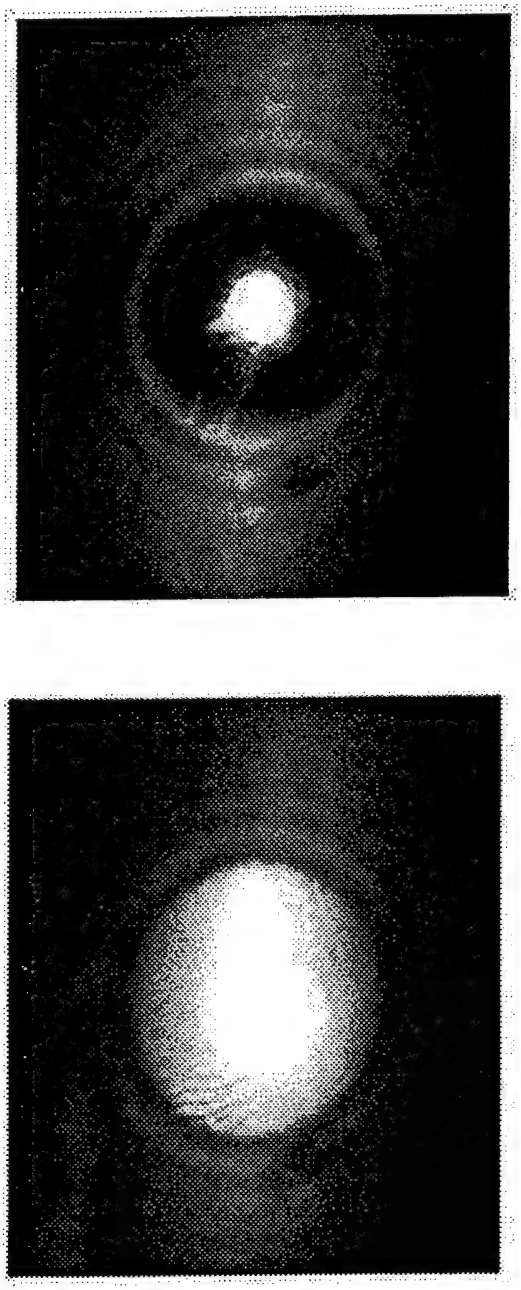

Figure 20. *(a) The transmitted light is shown for the condition where the crystal is in a low transmission state. The central spot is the transmitted laser while the surrounding black disk is the Kossel ring. (b) Same as (a) except the crystal is now in a high transmission state.*

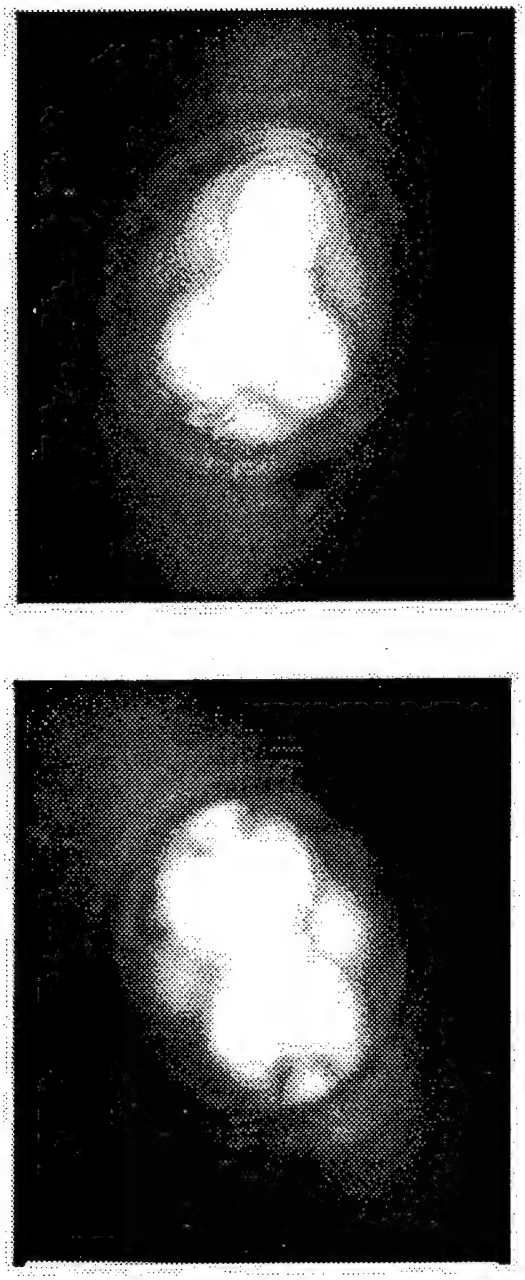

Figure 21. *The spatial distribution of the transmitted laser beam for the case when the system is in the (a) second highly transmitting state and (b) third highly transmitting state.*

II.E. Pump-Probe Measurements

To further characterize the interaction of the light with the colloidal crystal under the conditions where we observe optical bistability we studied the transmission spectrum with a weak probe laser when the crystal was illuminated by a strong pump laser. Figure 22 shows the experimental apparatus used for these measurements. The measurement was performed using two counterpropagating beams from two separate dye lasers. The first laser was used to switch the crystal to a high transmission state while the second laser, which was much weaker, was used to measure the transmission spectrum of the crystal. The plane of polarization of the probe beam was adjusted to be perpendicular to that of the pump beam so that polarization techniques could be used to separate the pump and probe light. In addition, to further discriminate between the pump and probe beams, the probe beam was chopped at a frequency of 2.5 kHz and a lockin amplifier was used to detect the transmitted light. The probe beam was focused to a spot size of ~5 μm at the sample. The pump beam was focused into the sample at the same location as the probe beam and had an intensity of approximately 60 kW/cm^2.

The low intensity transmission spectrum without the presence of the pump beam was recorded first. The transmission spectrum recorded is shown in Fig.23(a). For this colloidal crystal the center of the stop gap was located at 589.75 nm. The solid line in Fig. 23(b) shows the transmission spectrum recorded in the presence of the strong pump laser that was tuned to a wavelength of 590.25 nm. The dashed line shows the spectrum recorded with no pump beam. From this data we see that the center of the stop gap shifted to a shorter wavelength in the presence of the strong pump beam as we would expect theoretically. In addition, there is some new structure present on the long wavelength side of the stop gap that includes a peak in the transmission coinciding with the wavelength of the pump laser.

The transmission spectrum taken when the wavelength of the pump beam was tuned to 588.75 nm (which is near the center of the stop gap) is shown by the solid line in Fig. 24(a). For this case the stop gap is much wider than the original stop gap. However the most dramatic feature is the sharp transmission peak located at the wavelength of the pump beam. Similarly as shown in Fig.

24(b), when the pump beam is tuned to 587.75 nm there is still a narrow transmission peak at the wavelength of the pump beam.

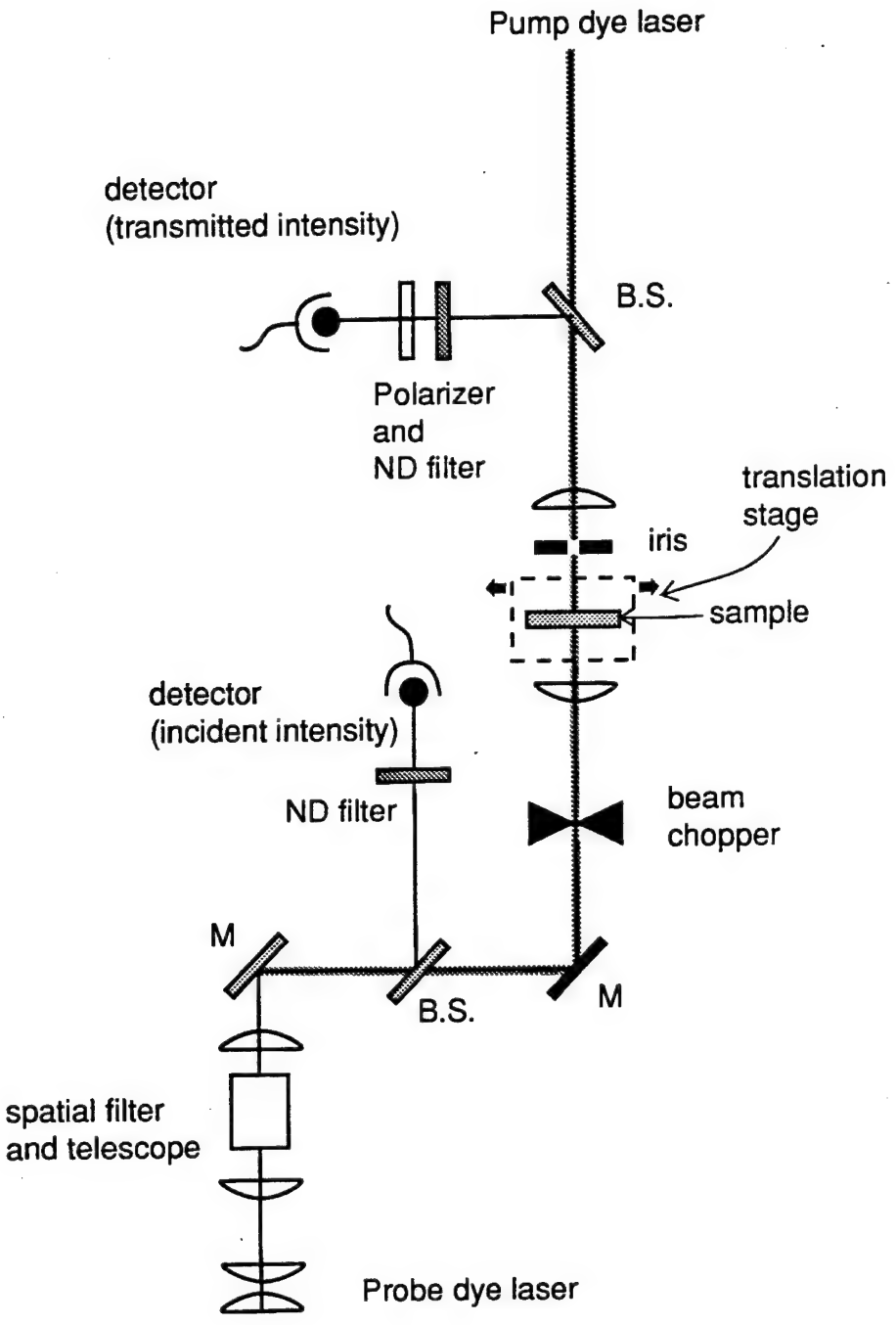

Figure 22. *Experimental setup used for the pump-probe experiments.*

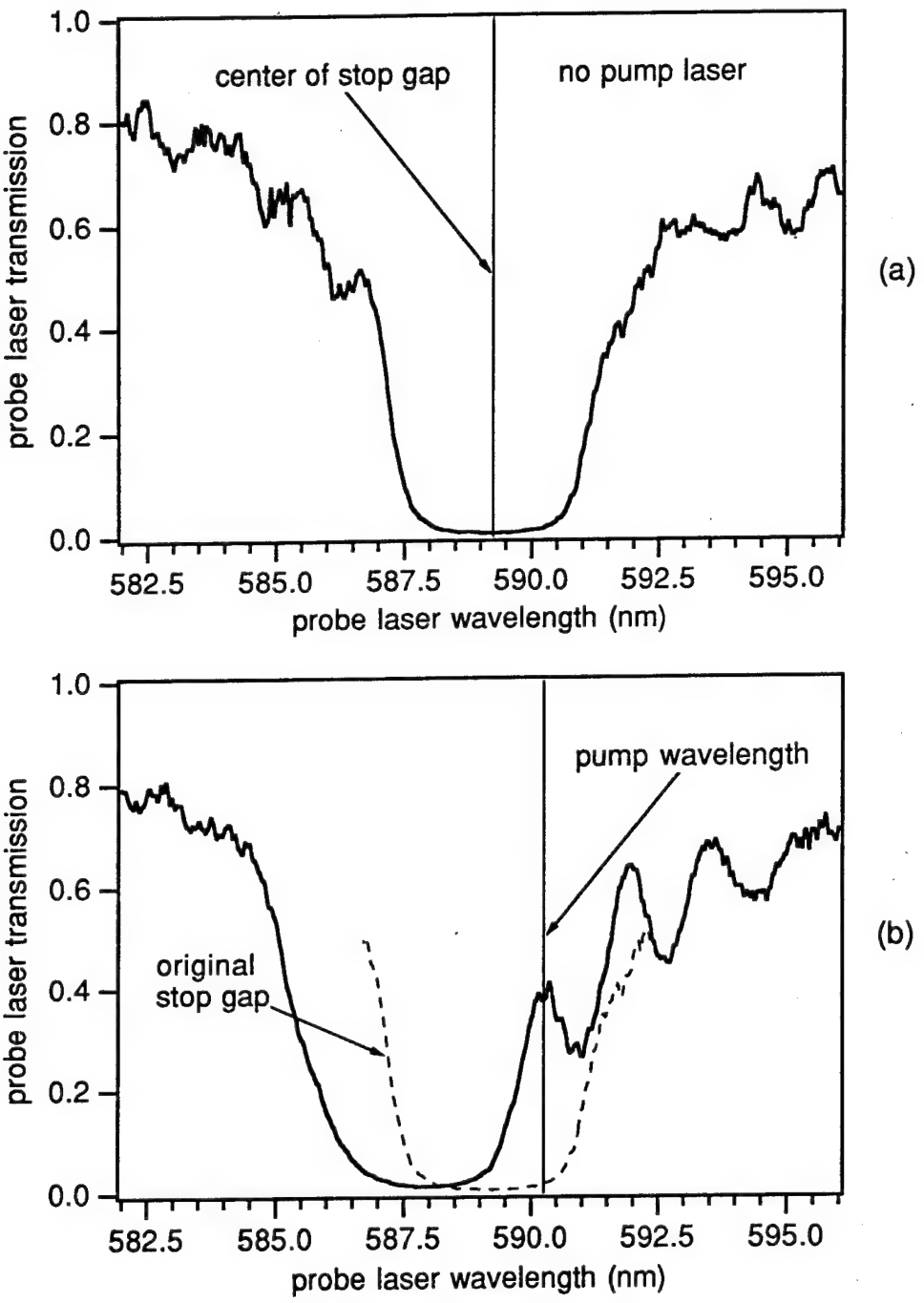

Figure 23. *The transmission spectrum is shown for (a) the case of no pump beam and (b) the case when the pump beam was tuned to 590.25 nm. The thin solid line indicates the wavelength of the pump beam while the dashed line represents the position of the original stop gap recorded with no pump beam.*

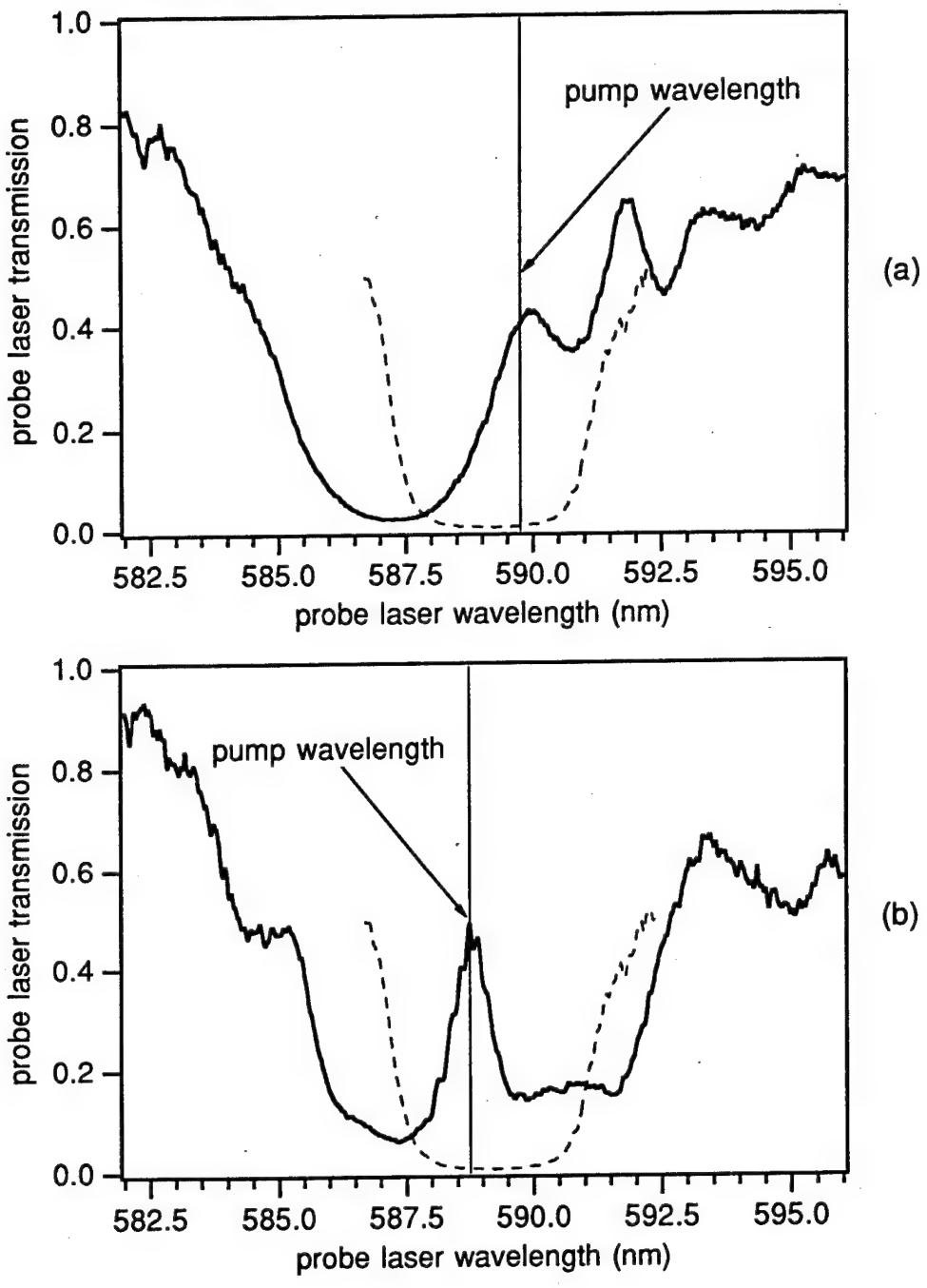

Figure 24. *The transmission spectrum is shown for (a) the pump beam tuned to 589.75 nm and (b) the pump beam tuned to 587.75 nm.*

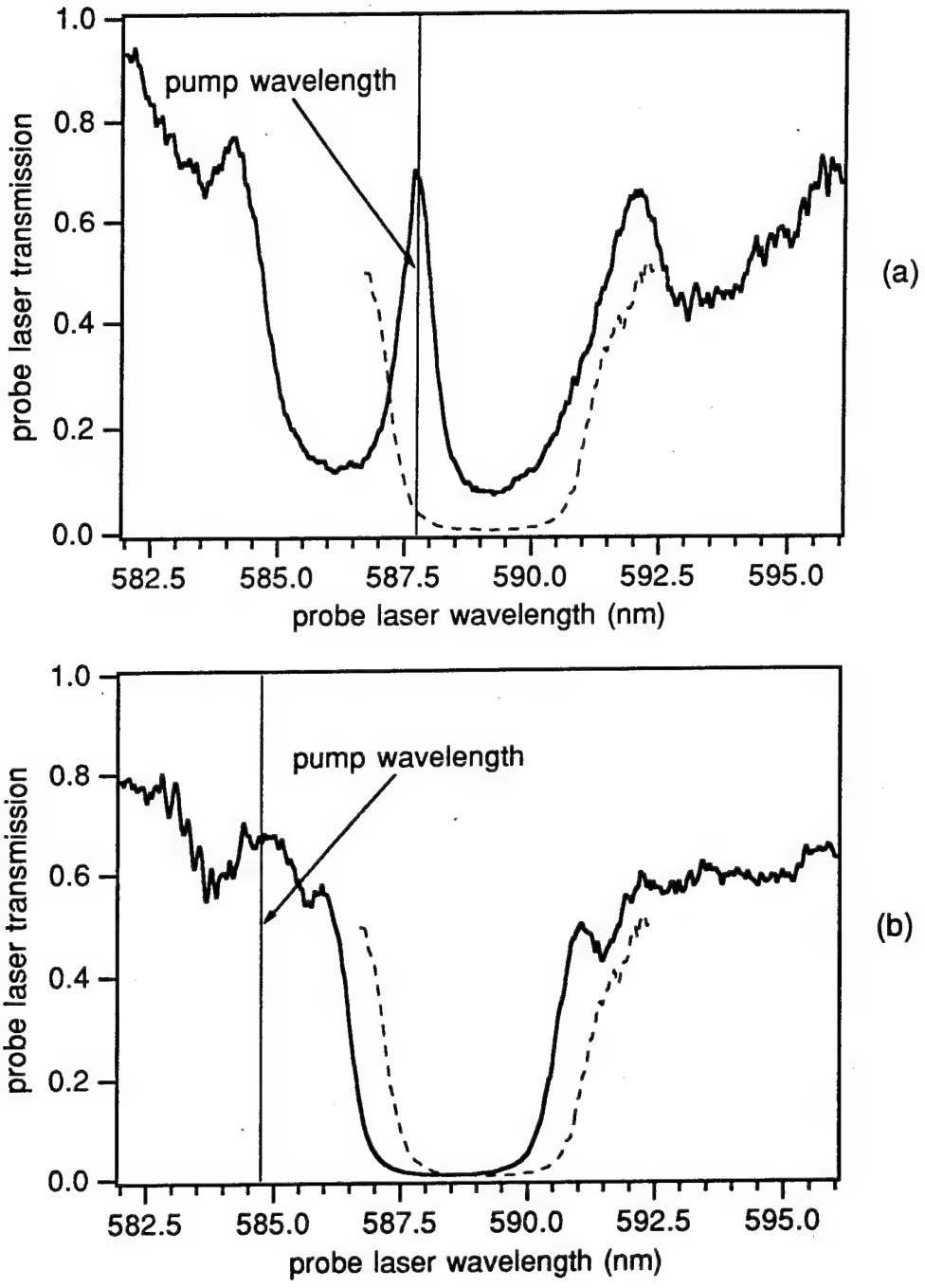

Figure 25. *The transmission spectrum is shown for (a) the pump beam tuned to 585.75 nm and (b) the pump beam tuned to 584.75 nm.*

When the pump laser is tuned to the blue edge of the stop gap we find that there is a much smaller modification to the transmission of the probe laser. Fig. 25(a) shows the spectrum recorded when the wavelength of the pump laser was tuned to 585.75 nm. When the pump laser is tuned even further to the blue (584.75 nm) we see almost no visible distortion in the stop gap and only a blue shift of the central wavelength, as shown in Fig. 25(b).

These pump-probe measurements demonstrate that the transmission of the colloidal crystal is dramatically modified in the presence of a strong pump beam and that this modification is strongly dependent on the wavelength of the pump laser. Two principal changes in the transmission spectra were found to take place. First, the center of the stop gap appears to shift to higher frequencies. Second, a large increase in transmission appears at wavelengths centered about the wavelength of the pump laser. The shift in the stop gap appears to support the theory presented in the previous section where the colloidal crystal compresses due to an electrostrictive force. As the lattice spacing decreases, the Bragg wavelength should decrease, producing a blue shift of the stop gap.

We don't feel that the sharp peak in the transmission can be explained by just a simple compression of the lattice. One explanation of this feature that seems possible is that there is enough force on the lattice to cause a discontinuous jump in the lattice periodicity. This kind of a discontinuity is often referred to as a defect [33]. A discontinuous jump in the lattice can dramatically modify the transmission spectrum of the periodic structure. Consider the simplest type of defect that can form where either an excess of dielectric material is added or dielectric material is removed from the center of the periodic structure. Each uniform period section behaves as a mirror that will reflect any light whose frequency falls within the stop gap of the structure. The phase slip between the two highly reflective sections acts as a Fabry-Perot cavity and the structure can be highly transmitting for some frequencies that were reflected for the case of a uniform DFBS. To demonstrate this point we calculated the transmission of a periodic structure with a quarter wavelength phase slip. The dashed curve in Fig. 26 is a plot of the transmission calculated using the coupled amplitude equations assuming quarter wavelength phase slip at the center of the structure, a coupling value of $\kappa L=3.5$, and $\Lambda=216$ nm. In addition to the

phase slip we have included a uniform compression of the lattice by 0.5% in the direction of propagation of the light. The solid line in Fig. 26 shows the experimentally measured transmission for the case when the pump laser was tuned to a wavelength of 588.25 nm. We can see that the phase slip results in a narrow transmission feature that is similar to what we see in our experimental measurements. The compression of the lattice results in the slight asymmetry that we see in the experiment.

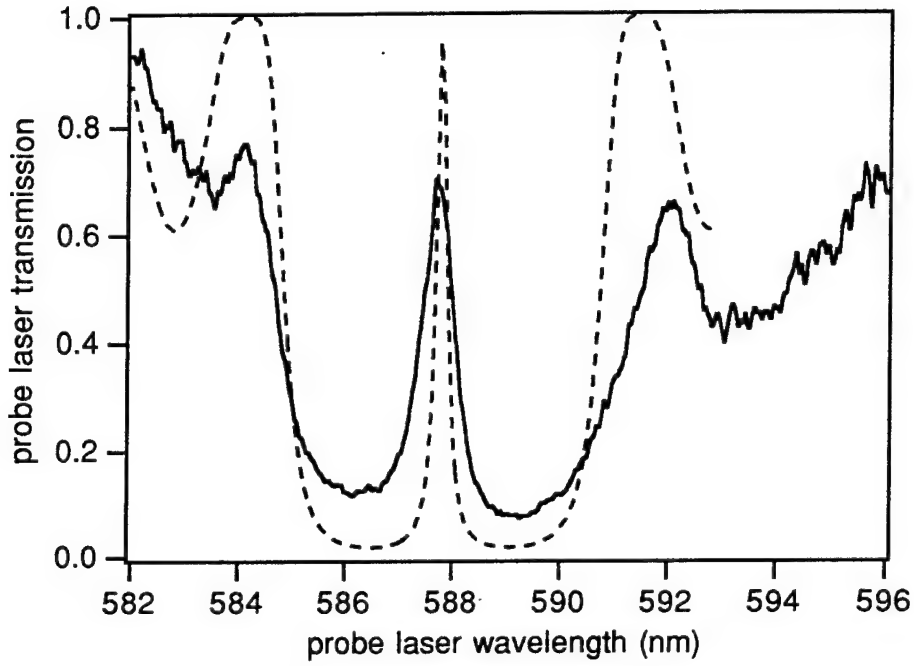

Figure 26. *The transmission spectrum for the case when the pump beam is tuned to 588.25 nm is shown by the solid line. The dashed line shows the calculated curve for the case of a quarter wavelength phase slip in the center of the structure.*

At this point we do not have definite proof that defect formation is responsible for the narrow feature in the transmission spectra. However many of the characteristics suggest that there is a phase slip in the periodic structure. More theoretical and experimental work is required to verify that this model is correct.

II.F. Temporal Instabilities

Temporal instabilities have been predicted and observed in many different nonlinear optical systems. Nonlinear ring cavities [34], nonlinear Fabry-Perot resonators [35], and counterpropagating beams in a Kerr medium [36] have all been shown to exhibit self-pulsing and optical chaos at high intensities. There has also been interest in temporal instabilities in the transmission of nonlinear DFBS. These structures are predicted to exhibit temporal fluctuations in the transmission light under certain conditions as were discussed in the first section of the document.

In our experiment, temporal fluctuations were observed when the incident intensity was increased above the range of intensities where optical switching was observed. At these intensities, a periodic fluctuation in the transmission was observed. We found that the onset of the self-oscillations occurred at a much lower intensity near the high frequency edge of the stop gap. We also found that the frequency of the oscillations ranged from about 20 to 700 kHz and depended on the specific sample, incident intensity and the frequency detuning from the center of the stop gap. In addition to the oscillations in the transmitted intensity the spatial pattern of the transmitted light also fluctuated.

The temporal fluctuations of the transmission of a colloidal crystal were studied as a function of intensity and detuning from the center of the stop gap. The data collected as a function of intensity were taken using a crystal whose stop gap was located near 514.5 nm. Therefore an argon ion laser was used in these experiments. The laser detuning was near the high frequency edge of the stop gap. Studying the temporal fluctuations over a large range of intensities was difficult because the intensities needed for the experiment were near the damage threshold of the crystals. The experimental setup used to characterize the temporal instability was the same as that used for the optical limiting or optical switching experiments. The samples were colloidal crystals made of suspensions of 120 nm polystyrene spheres.

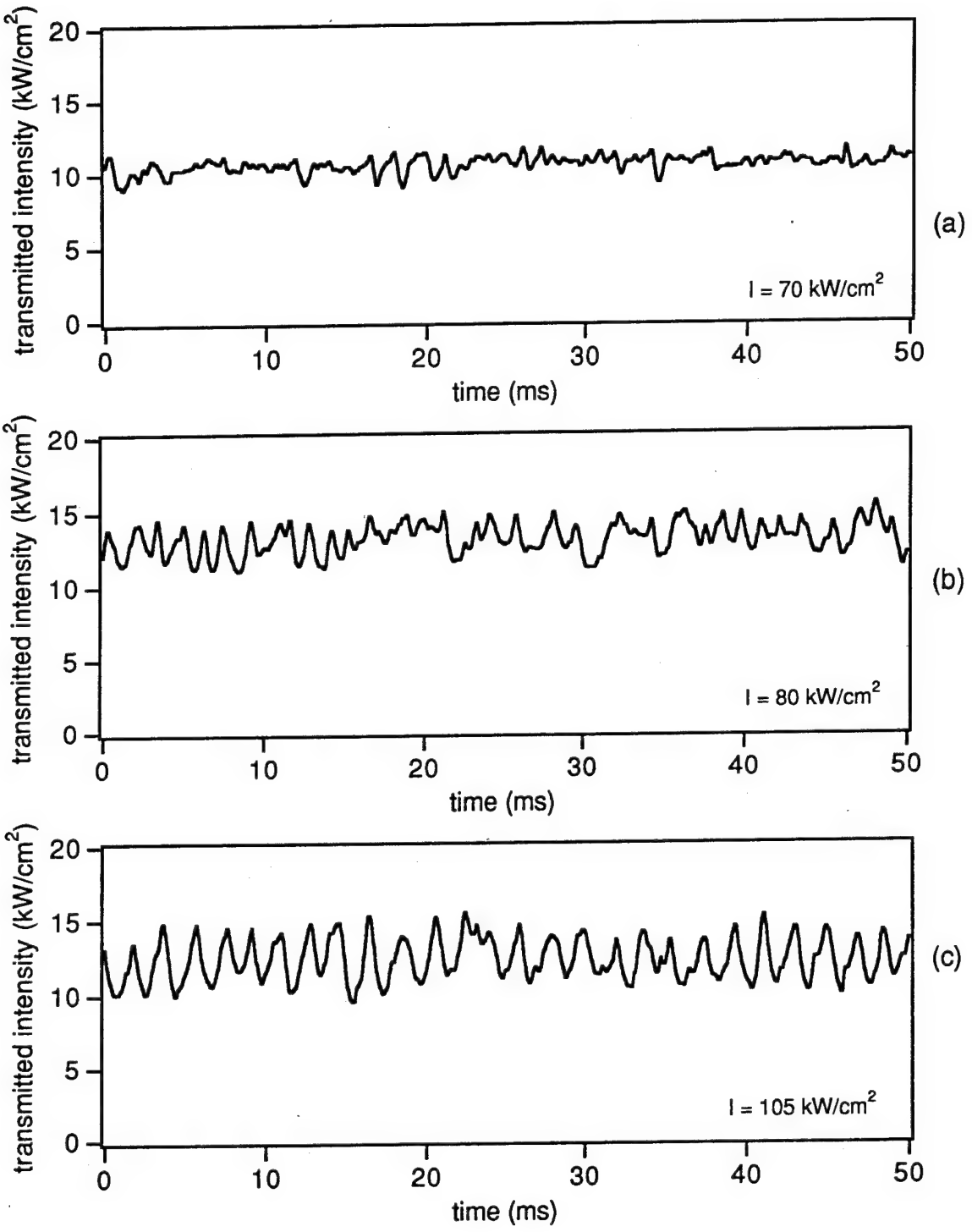

Figure 27. *Transmission of the colloidal crystal plotted as a function of time. The wavelength of the incident laser beam is tuned to the high frequency edge of the stop gap. The incident intensity is (a) 70 kW/cm^2, (b) 80 kW/cm^2 and (c) 105 kW/cm^2.*

At intensities below 50 kW/cm^2, the sample appeared to be in the low transmission state and no temporal fluctuations were observed in the transmitted light. For an intensity between 50 and 70 kW/cm^2 the sample appeared to switch to a high transmission without any temporal instability. Above 70 kW/cm^2 temporal fluctuations began to appear in the transmitted light, as shown in Fig. 27(a). At an intensity of 80 kW/cm^2 the fluctuations appeared to be somewhat periodic and the using fourier analysis the dominant oscillation frequency was found to be 630 Hz (Fig. 27(b)). More distinct oscillations were observed as the incident intensity was increased. Fig. 27(c) is a plot of the transmitted intensity for an incident intensity of 105 kW/cm^2. The dominant oscillation frequency in this case is about 515 Hz. As the incident intensity was increased further, as shown in Figs. 28(a-c), the oscillation frequency continued to decrease. Beyond an intensity of 200 kW/cm^2 the fluctuations appeared to cease.

To study the characteristics of the temporal fluctuations as a function of detuning we used a tunable dye laser and a colloidal crystal with a stop gap centered at approximately 580.0 nm. The low intensity transmission spectrum for the crystal is shown in Fig. 29. The transmission of the sample exhibited bistability when the wavelength of the incident light was tuned to the center of the stop gap. The transmission appeared to switch to a high state when the incident intensity was between 40 and 60 kW/cm^2. Temporal fluctuations were not observed when the wavelength of the incident light was longer than 580.4 nm. Fig. 30(a) is a plot of the transmission of the crystal as a function of time for a wavelength of 580.4 nm. The incident intensity was held constant at 80 kW/cm^2. As the laser was tuned to higher frequencies, the frequency of the oscillations increased. Fig. 30(b) is a plot of the data recorded at a wavelength of 579.7 nm and Fig. 30(c) shows the time dependent transmission for a wavelength of 579.2 nm. Figs. 31 shows the temporal behavior of the transmission as the wavelength of the laser is tuned further towards the blue. From these graphs we can see that the decreases as a function of decreasing wavelength.

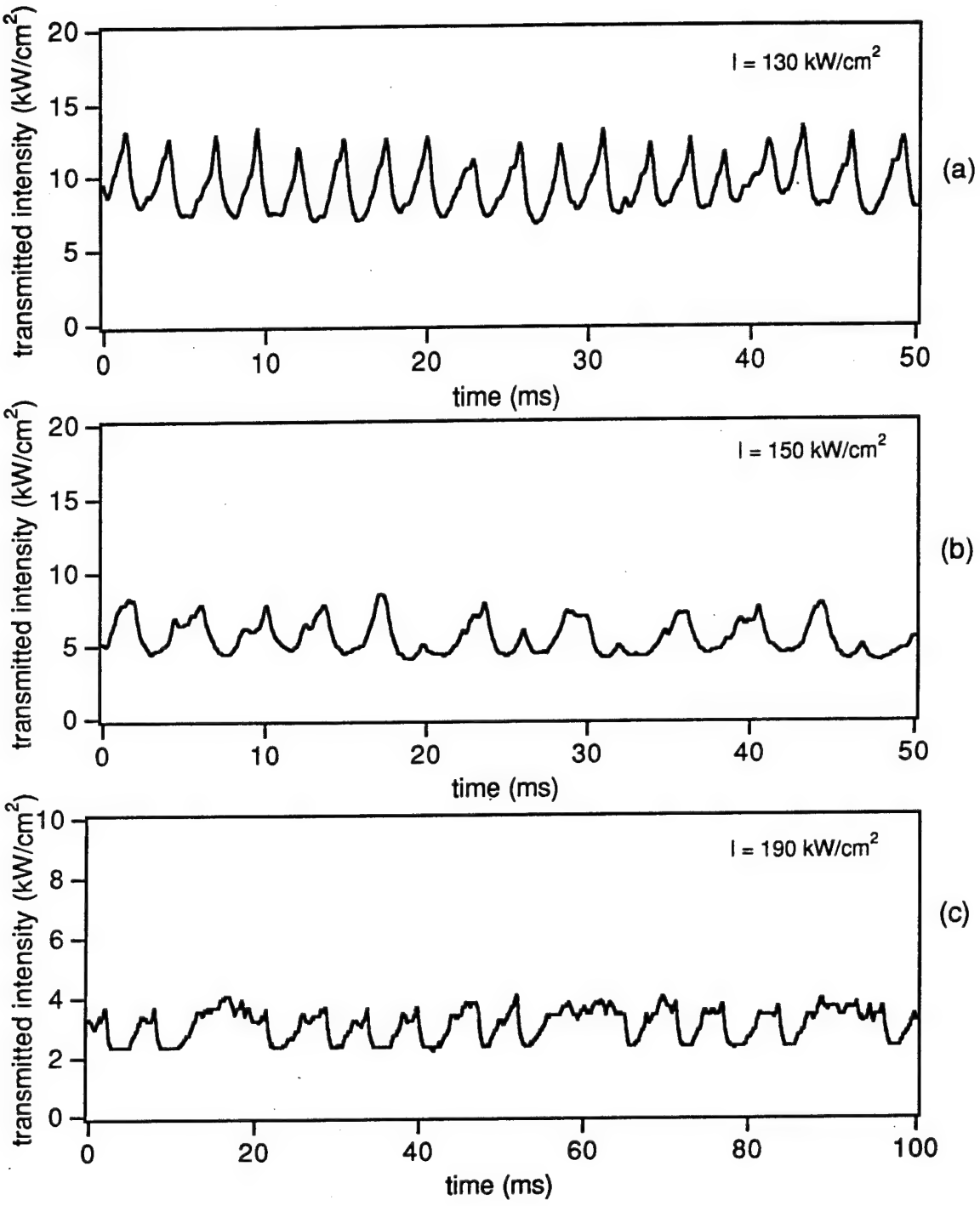

Figure 28. *Transmission of the colloidal crystal plotted as a function of time. The incident intensity is (a) 130 kW/cm^2, (b) 150 kW/cm^2 and (c) 190 kW/cm^2.*

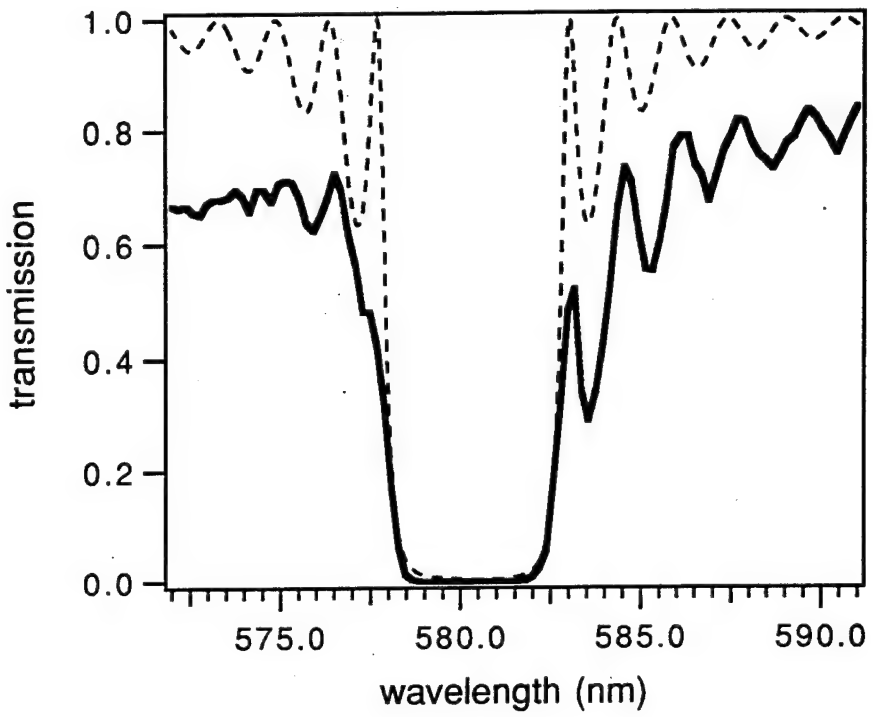

Figure 29. *Transmission spectrum of the colloidal crystal used to study the wavelength dependence of the temporal instabilities. The solid line shows the experimental measurements and the dashed line shows the theoretical fit.*

At this time we do not have a working model of the temporal instability in the colloidal crystal system. This system differs significantly from the nonlinear DFBS modeled previously. The nonlinearity of the system is not a simple Kerr nonlinearity and the response time of the nonlinearity is much longer than the transit time through the crystal. Further experimental work and theoretical modeling as needed to understand the origin of the temporal fluctuations.

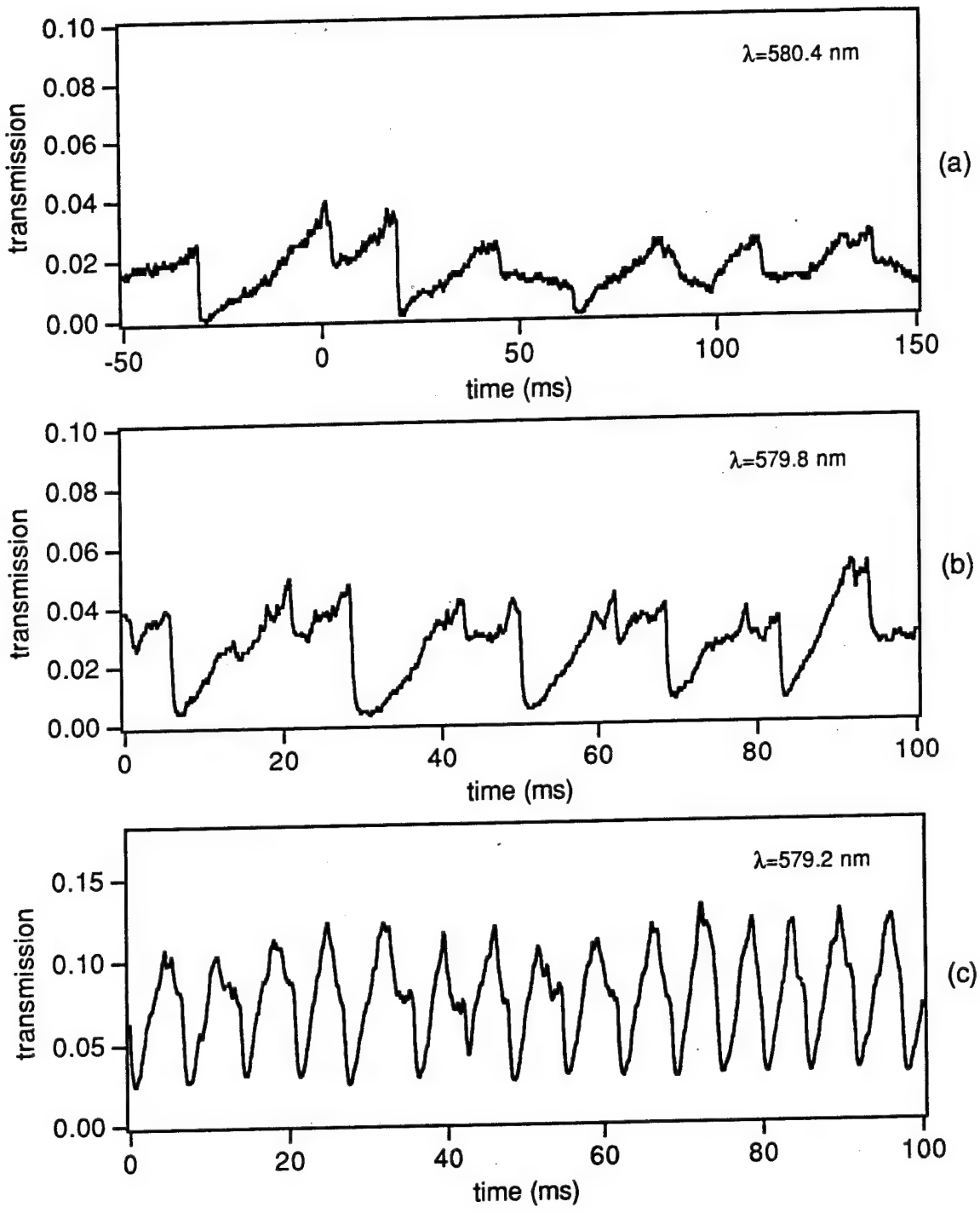

Figure 30. *The temporal dependence of the transmission of the colloidal crystal for an incident intensity of 80 kW/cm^2 and an wavelength of (a) 580.4 nm, (b) 579.8 nm and (c) 579.2 nm.*

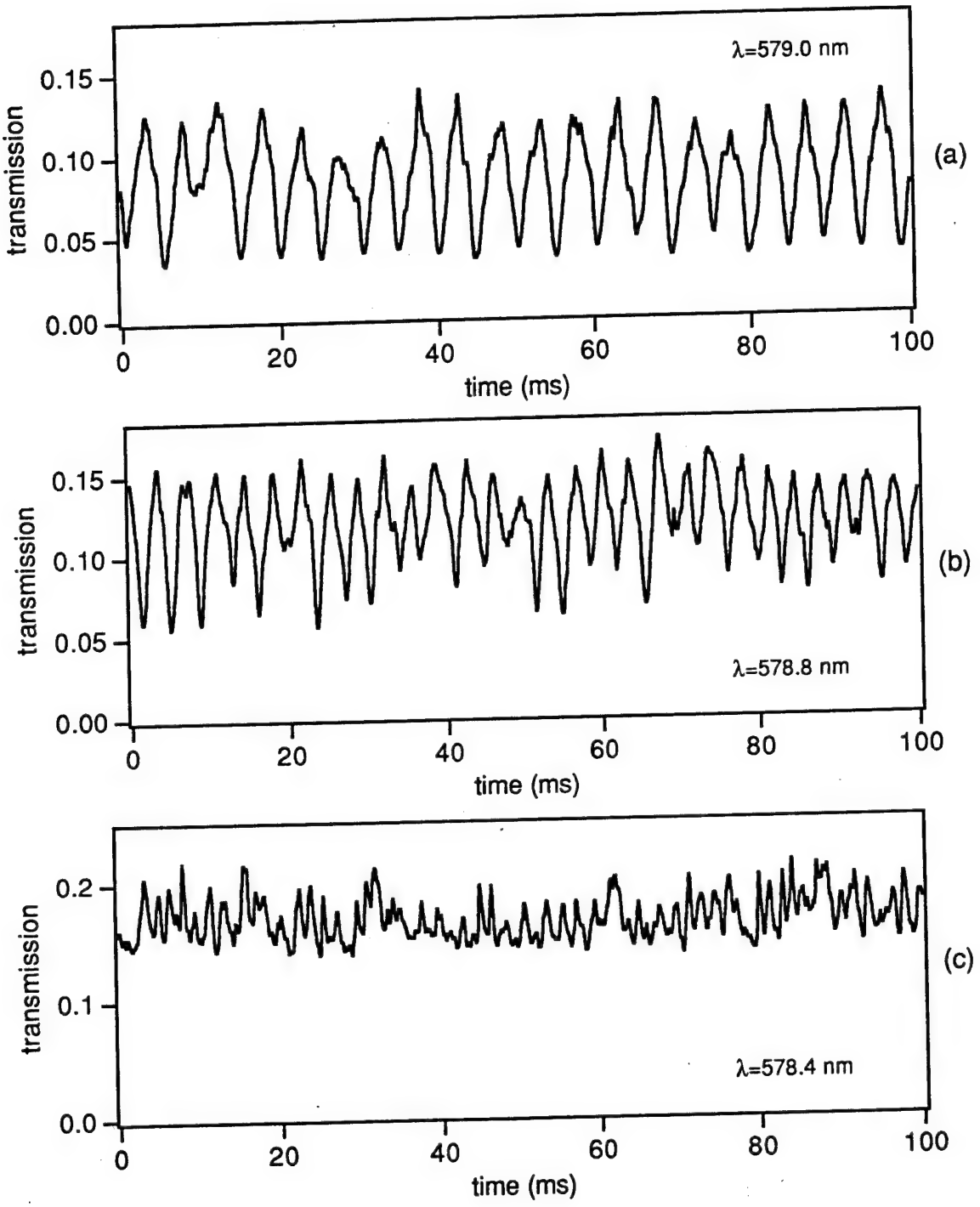

Figure 31. *The temporal dependence of the transmission of the colloidal crystal for an incident intensity of 80 kW/cm^2 and an wavelength of (a) 579.0 nm, (b) 578.8 nm and (c) 578.4 nm.*

III. Switchable Gratings

Diffractive optical elements with diffraction efficiency that can be controlled in real time are under investigation for use in reconfigurable optical interconnects, machine vision, image processing, and many other applications. Recent work has concentrated on methods to electrically switch the diffraction efficiency of holographic optical elements, which can be used to redirect beams of light. Diffraction gratings recorded in polymer dispersed liquid crystals [37], DMP-128 gratings imbibed with a nematic liquid crystal [38,39], liquid crystal/surface relief hologram combinations [40,41], and liquid crystalline photopolymers [42] have been used as electrically switched elements. We present results that demonstrate optical control of the diffraction efficiency of volume holographic optical elements. Polaroid Corporation's DMP-128 was used to form the host gratings. These gratings were imbibed with the nematic liquid crystal 5CB, which was chosen for its relatively low clearing temperature. A thermal nonlinearity of the liquid crystal was utilized to achieve the switching behavior.

Volume phase transmission gratings were recorded with a spatial frequency of 1580 mm^{-1} by exposing the DMP-128 photopolymer to the interference pattern produced by two plane waves of wavelength 0.6328 μm. Each plane wave subtended an angle of 30° from the recording plane normal and were incident symmetrically on opposite sides of the normal. The exposure of these gratings was varied to maximize the diffraction efficiency of the first diffracted order after the grating was imbibed with the nematic liquid crystal.

Once the DMP-128 gratings are processed they are porous. To imbibe the gratings they were coated with 5CB liquid crystal, covered with a thin glass plate, and heated on a hot plate. At a temperature of approximately 35° C the grating became transparent. At this temperature the liquid crystal becomes isotropic with an index of refraction of 1.57 - 1.60 [43,44] Since the index of refraction of the DMP-128 is approximately 1.57 [38,39] the refractive index modulation of the grating is nearly eliminated at this temperature. The clearing and reappearing of the grating are reversible and many cycles were observed without variation.

A pair of OFF and ON states of the diffractive element can be attained several different ways. To illustrate the different methods we have calculated the normalized diffraction efficiency as a function of refractive index modulation for a 60 μm thick grating using the method of thin grating decomposition [45]. The results of this calculation are shown in Fig. 32. Fig. 32 shows that increasing index modulation results in many cycles of maximal and null diffraction efficiency, which is expected since the calculation was done for the quazi-Bragg regime. The figure shows that peak efficiencies in the high modulation maxima begin to decrease slightly. This is expected since the grating is not deep within the Bragg regime [46]. In one case, if any of the refractive indices n_o, n_e, or n_i of the liquid crystal closely match the index of refraction of the bulk DMP-128 material, then the liquid crystal exhibiting that index can effectively eliminate the spatially varying modulation of the composite grating. This zero modulation is shown as point (a) in Fig.32. When the liquid crystal is switched to one of the other orientations or states, the mismatch in index between the liquid crystal and photopolymer grating can be used with an optimized exposure (which controls the degree of porosity of the grating and hence modulation) to maximize the diffraction efficiency as shown by points (b) and (d) in the figure. If a close match is not available between the liquid crystal and photopolymer indices, then a second technique can be used in which the grating modulation is never zero, but is switched between high efficiency [e.g., points (b) or (d)] and zero efficiency [e.g., point (c)].

In this experiment the thermal nonlinearity of the liquid crystal [43] was utilized to switch the diffraction efficiency. Below the clearing temperature the liquid crystal is in the nematic state (n_e=1.74-1.67, n_o=1.54-1.51) and exhibits a refractive index different from that of the DMP-128 host (n_{DMP}~1.57). Above the clearing temperature, however, the liquid crystal becomes isotropic and exhibits a refractive index (n_i=1.60-1.57), which is close to that of the DMP-128 host. At temperatures near the nematic-isotropic phase transition a small change in temperature can produce a relatively large change in grating modulation, and a corresponding large change in diffraction efficiency.

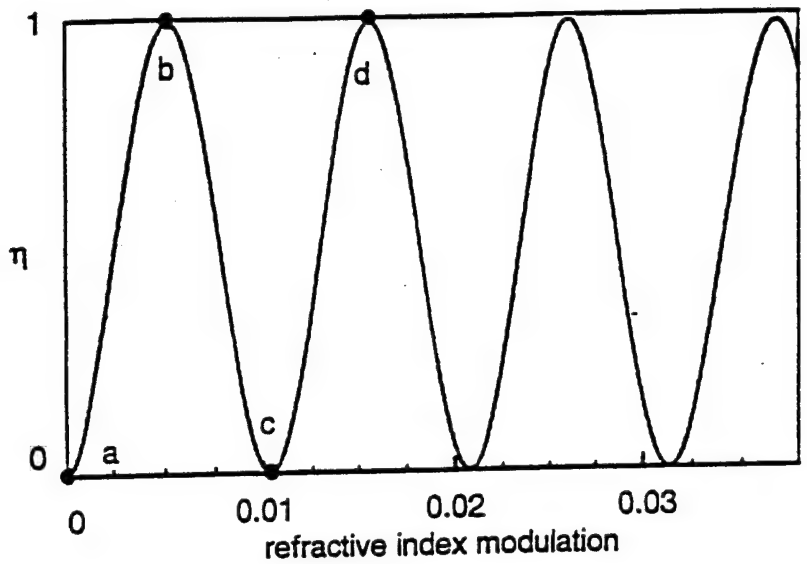

Figure 32. *Normalized diffraction efficiency as a function of refractive index modulation for a 60 μ m thick simusoidal phase grating. The theoretical curve was calculated using thin grating decomposition. Grating switching can be obtained between peak values (b, d, etc.) and either zero modulation or nonzero modulation values (e.g., c) that result in minimal diffraction efficiency.*

The thermal nonlinearity was characterized by measuring the diffraction efficiency of the liquid crystal composite grating as a function of temperature. The composite grating was mounted inside an oven whose temperature could be controlled between room temperature and 40° C. Figure 33 shows the diffraction efficiency that was measured using a helium-neon laser operating at a wavelength of 0.6328 μm. The diffraction efficiency was seen to initially decrease as the temperature was increased, and then the diffraction efficiency increased as the temperature was increased further. From this result we can see that the grating modulation at room temperature was greater than that necessary for 100% diffraction efficiency. As the temperature of the liquid crystal is increased from 25° C to just below 35° C (the clearing temperature of the 5CB liquid crystal), n_o changes from 1.52 to 1.53 and n_e changes from 1.68 to 1.65. This change in index of the nematic liquid crystal results in enough index modulation change to modulate the diffraction efficiency from high to low. For the grating used in this experiment, the exposure was adjusted so that a maximum in diffraction efficiency occurs near the clearing temperature of the liquid crystal. When the composite grating is heated above the clearing temperature of 35° C, the liquid crystal

undergoes a phase transition to the isotropic state. In this state the index of refraction of the liquid crystal is very close to the index of refraction of the photopolymer and hence the index modulation is close to zero, which results in low diffraction efficiency. For the optical switching experiment the composite grating was heated to a temperature of between 34.4° C and 34.8° C. In this range only a small temperature change is required to produce a large change in the index of refraction of the liquid crystal and a corresponding large change in diffraction efficiency.

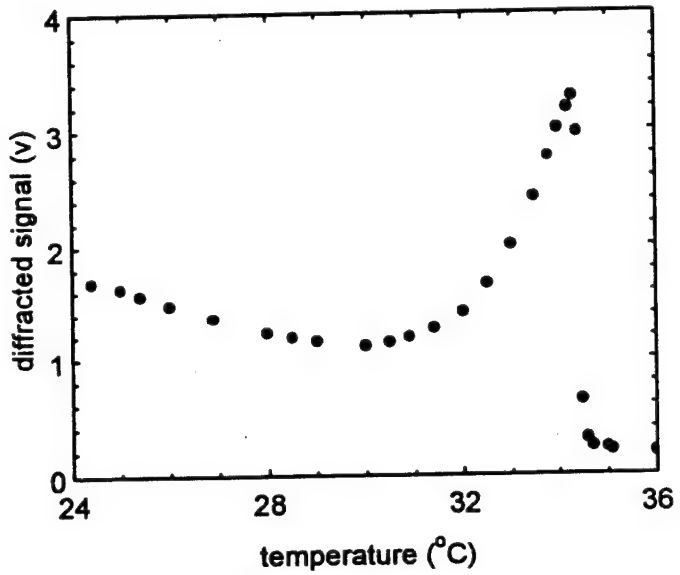

Figure 33. The temperature dependence of the diffraction efficiency.

The optical switching experimental configuration is illustrated in Fig. 34. A small region of about 20 μm^2 on the composite grating was illuminated with a focused helium-neon laser beam. This beam acted as a probe to measure the diffraction efficiency of the grating. Also incident on the same region of the grating region, but from the opposite side of the element and in a counterpropagating direction as shown in Fig. 34 was a focused beam with a wavelength of 0.5145 μm from an argon ion laser. This beam illuminated a slightly larger area of the grating than the probe beam. The diffracted portion of the probe beam was detected after it passed through an interference filter (with a transmission peak centered at λ=0.6328 μm) which was used to isolate the probe beam from any of the green control beam that was scattered or reflected from the sample. The control beam was modulated by a chopper, and the detected signal was recorded

by a digital oscilloscope. For this experiment, a small amount of Rhodamine 6G dye was added to the liquid crystal before imbibing the grating. The resulting composite then exhibited on the order of one percent absorption at a wavelength of 0.5145 μm, while negligible absorption was observed at a wavelength of 0.6328 μm. During the experiment the sample was placed inside an oven that was used to bias the temperature of the nonlinear grating near the clearing temperature of the liquid crystal. The experimental results of the switching behavior at a temperature of 34.7 °C and control (argon ion laser) beam power of 8.4 mW are shown in Fig. 35. The diffraction efficiency is switched between high and low states with a time constant (1/e) of 0.9 ms.

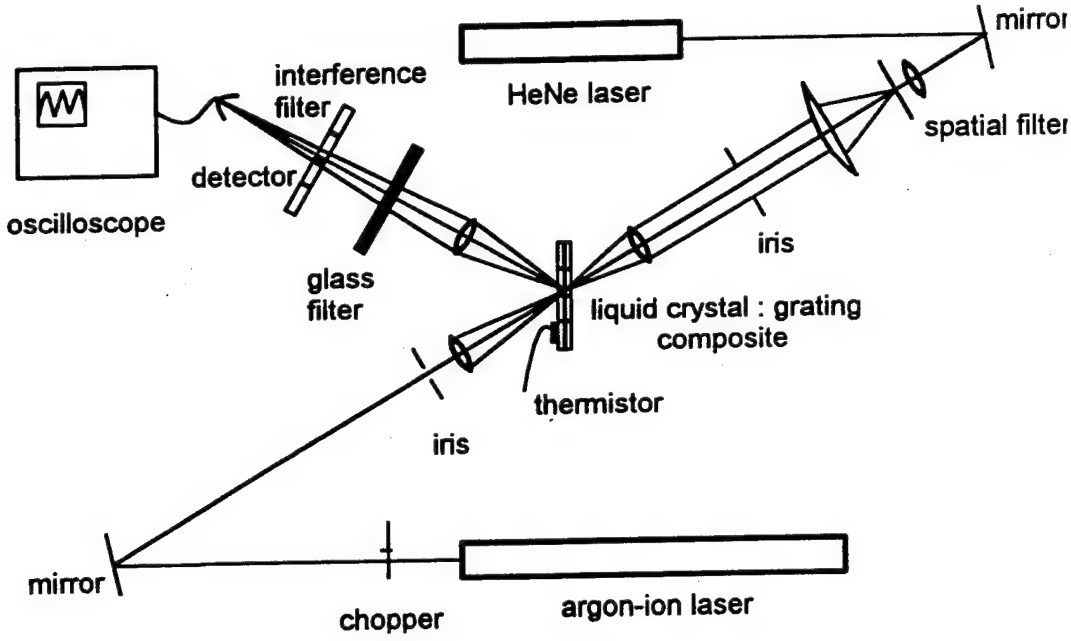

Figure 34. *Experimental setup used to measure the modulated diffraction efficiency of the composite gratings. A control beam from an argon ion laser was used to switch the diffraction efficiency of a small region of the nonlinear composite grating. The beam from a helium-neon laser was used to monitor the diffraction efficiency.*

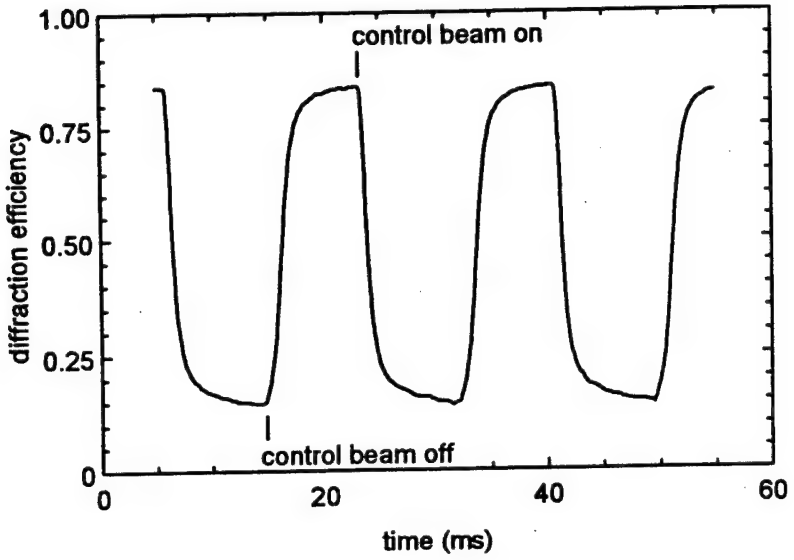

Figure 35. *Optically controlled switching of the diffraction efficiency of the composite grating for a control beam power of 8.4 mW. The diffraction efficiency is switched between high and low values with the absence or presence of an optical control beam, respectively.*

Experimental results of the switching behavior at various bias temperatures are shown in Fig. 36. The diffraction efficiency is plotted as a function of time with a control (argon ion laser) beam power of 8.4 mW. At a constant control beam power, as the bias temperature of the composite grating is increased the depth of modulation of diffraction efficiency increases, which can be seen by comparing curves (a) - (c) of Fig. 36. However as the bias temperature is increased closer to the clearing temperature the depth of modulation decreases as the liquid crystal apparently never fully recovers to the nematic state. Hence the peak diffraction efficiency at these temperatures is much lower as can be seen in curves (d) and (e) of Fig. 36.

Figure 37 is a plot of the diffraction efficiency vs. time for a bias temperature of 34.4° C. We chose this temperature since it is as far from the clearing temperature as we can go before the diffraction efficiency with no control beam starts to drop. At this temperature a higher control beam power is required to obtain nearly 100% modulation of the diffraction efficiency.

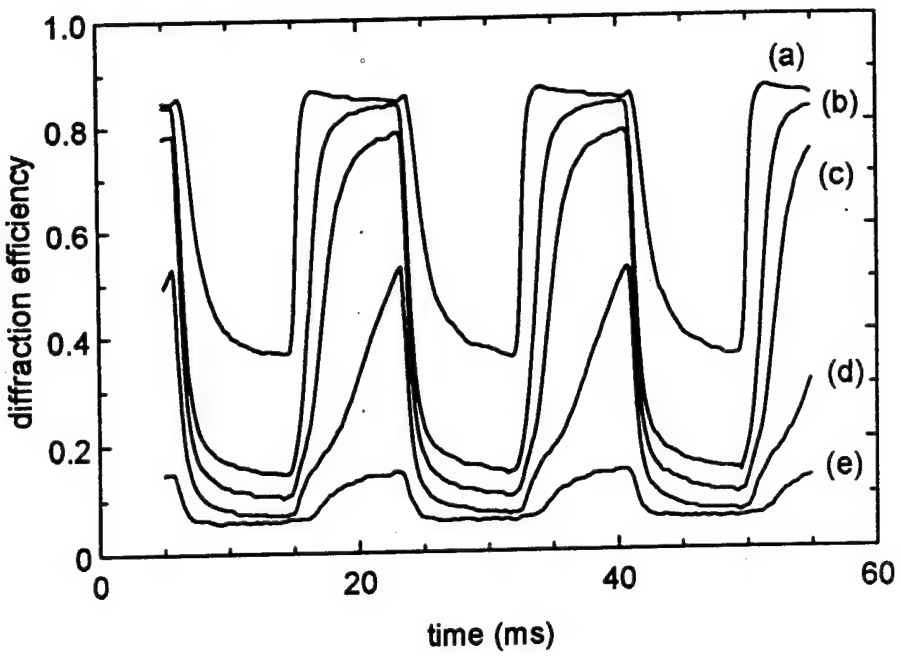

Figure 36. *Optically controlled switching of the diffraction efficiency of the composite grating for a control beam power of 8.4 mW. The diffraction efficiency is switched between high and low values with the absence or presence of an optical control beam, respectively. The five curves are taken at bias temperatures of (a) 34.4° C, (b) 34.7° C, (c) 34.8° C, (d) 34.9° C, and (e) 35° C.*

In the context of beam steering, the optical switching mechanism that we have investigated has many desirable features. For example the wavelength of the control beam can be well removed from that of the signal beam, and thus spurious signals are easily blocked. Since the native absorption of the pure liquid crystals is negligible in the visible and near infrared, a multitude of signal and control wavelengths can be accommodated by proper choice of the dye used. Further, since the absorption feature is typically only on the order of 100 nm broad, many different signal wavelengths or broadband signal beams can be used. Although in this experiment a relatively low switching power of 8 mW per channel is demonstrated, these results were obtained with a very low absorption of the control beam (on the order of one percent). As this absorption is increased by increasing the dye concentration we expect that this switching power may be reduced significantly, perhaps to the microwatt regime. Any decrease in switching power required per channel will be particularly valuable since we are nearly in the regime where scaleable arrays of

microlasers (e.g., vertical cavity surface emitting lasers, VCSELs) can be used as the source of control beams.

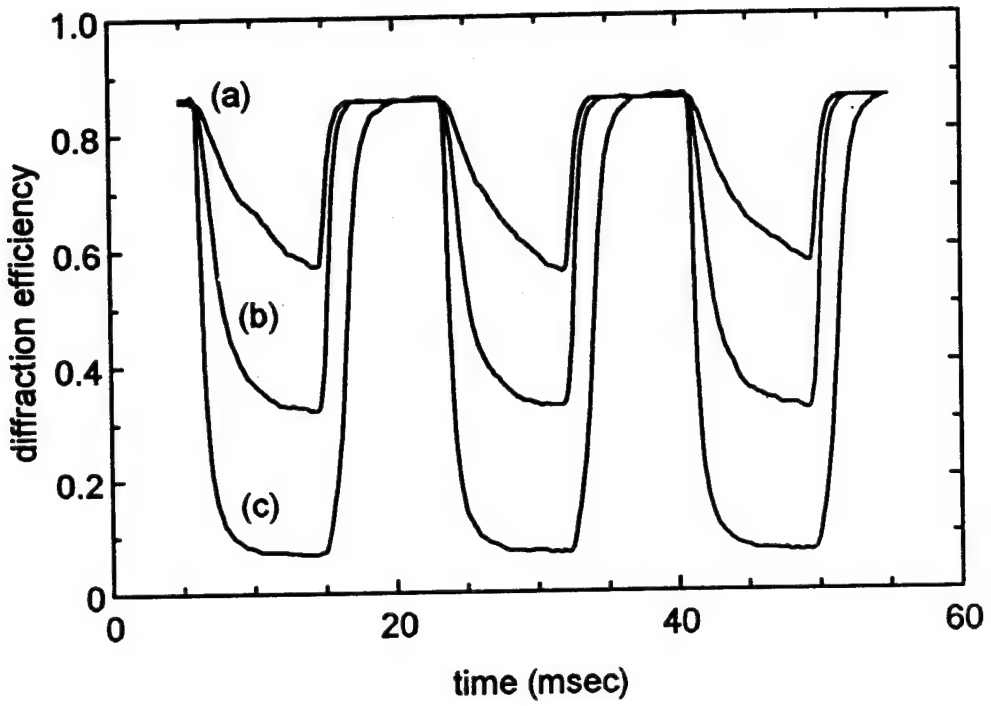

Figure 37. *Optically controlled switching of the diffraction efficiency of the composite grating at a bias temperature of 34.4° C. The three curves are recorded at control beam powers of (a) 9.5 mW, (b) 12.6 mW, and (c) 49.6 mW.*

IV. Conclusions

In this work we have studied the optical properties of nonlinear periodic structures. Two experimental systems have been studied: colloidal crystals and photopolymer/liquid crystal composite gratings. The colloidal crystals were used as nonlinear distributed feedback structures. The transmission of the colloidal crystal was seen to display optical limiting, optical switching and bistability, and temporal instabilities. We found that the switching intensity decreased as the frequency of the incident light was tuned deeper within the stop gap. This dependence can not be explained by the simple theory of nonlinear distributed feedback structures. Further work is needed to explain this result. In addition, a narrow spectral feature in the transmission spectrum

was observed in a pump-probe experiment. This narrow spectral feature also can not be explained by the simple theoretical models. More experimental and theoretical work is needed to explain this spectral feature and to determine whether this feature is related to the decrease in the switching intensity.

We have observed optical switching of the diffraction efficiency of a volume holographic optical element. The nonlinear grating consisted of a grating recorded using Polaroid Corporation's DMP-128 photopolymer that was filled with 5CB nematic liquid crystal. A thermal nonlinearity of the liquid crystal was utilized. Nearly 100% modulation of the diffraction efficiency was achieved with a control beam power of less than 10 mW. The time response of the switching was measured to be less than 1 ms. Further work is needed to investigate the potential for reducing the switching power requirements by increasing the dye concentration in the liquid crystal. In addition, future work that investigates the doping of other nonlinear materials into the composite gratings would be useful. The use of other nonlinear materials would make a faster response time possible.

V. References

1. C. J. Herbert, W. S. Capinski, and M. S. Malcuit, "Optical Power Limiting with Nonlinear Periodic Structures," *Opt. Lett.* **17**, 1037 (1992).
2. C. J. Herbert and M. S. Malcuit, "Optical Bistability in Nonlinear Periodic Structures," *Opt. Lett.* **18**, 1783 (1993).
3. M. S. Malcuit and C. J. Herbert, "Optical Properties of Nonlinear Periodic Structures," *Acta Physica Polinica A* **86**, 127 (1994).
4. M. S. Malcuit and T. W. Stone, "Optically Switched Volume Holographic Elements," *Opt. Lett.* **20**, xxx (1995).
5. H. G. Winful, J. H. Marburger, and E. Garmire, "Theory of Bistability in Nonlinear Distributed Feedback Structures," *Appl. Phys Lett.* **35**, 379 (1979).
6. H. G. Winful, "Nonlinear Reflection in Cholesteric Liquid Crystals: Mirrorless Optical Bistability," *Phys. Rev. Lett.* **49**, 1179 (1982).

7. G. Assanto and G. I. Stegeman, "Optical Bistability in Nonlocally Nonlinear Periodic Structures," *Appl. Phys. Lett.* **56**, 2285 (1990).

8. P. A. Gohman, G. Bambakidis, and R. J. Spry, "Theoretical Intensity-Dependent Response of Nonlinear Periodic Structures," *J. Appl. Phys.* **67**, 40 (1989).

9. J. He and M. Cada, "Optical Bistability in Semiconductor Periodic Structures," *IEEE J. Quantum Elect.* **QE-27**, 1182 (1991).

10. H. G. Winful and G. D. Cooperman, "Self-Pulsing and Chaos in Distributed Feedback Bistable Optical Devices," *Appl. Phys. Lett.* **40**, 298 (1982).

11. C. M. de Sterke and J. E. Sipe, "Coupled Modes and the Nonlinear Schrodinger equation," *Phys. Rev. A* **42**, 2858 (1990).

12. H. G. Winful, R. Zamir, and S. Feldman, "Modulational Instability in Nonlinear Periodic Structures: Implications for Gap Solitions," *Appl. Phys. Lett.* **58**, 1001 (1991).

13. C. M. de Sterke, "Stability Analysis of Nonlinear Periodic Structures," *Phys. Rev. A* **45**, 8252 (1992).

14. H. G. Winful, "Pulse Compression in Optical Fiber Filters," *Appl. Phys. Lett.* **46**, 527 (1985).

15. W. Chen and D. L. Mills, "Gap Solitons and the Nonlinear Optical Response of Superlattices," *Phys. Rev. Lett.* **58**, 160 (1987).

16. J. E. Sipe and H. G. Winful, "Nonlinear Schrodinger Solitons in a Periodic Structure," *Opt. Lett.* **13**, 132 (1988).

17. C. M. de Sterke and J. E. Sipe, "Envelope-Function Approach for the Electrodynamics of Nonlinear Periodic Structures," *Phys. Rev. A* **38**, 5149 (1988).

18. C. M. de Sterke and J. E. Sipe, "Self-Localized Light: Launching of Low-Velocity Solitons in Corrugated Nonlinear Waveguides," *Opt. Lett.* **14**, 871 (1989).

19. D. N. Christodoulides and R. I. Joseph, "Slow Bragg Solitons in Nonlinear Periodic Structures," *Phys. Rev. Lett.* **62**, 1746 (1989).

20. R. L. Sutherland, "Bragg Scattering in Permanent Nonlinear Particle Gratings," *J. Opt. Soc. Am. B***8**, 1516 (1991).

21. H. Kogelnik and C. V. Shank, "Coupled-Wave Theory of Distributed Feedback Lasers," *J. Appl. Phys.* **43**, 2328 (1972).

22. H. Stoll and A. Yariv, "Coupled-Mode Analysis of Periodic Dielectric Waveguides," *Opt. Commun.* **8**, 5 (1973).

23. N. D. Sankey, D. F. Prelewitz, and T. G. Brown, "All Optical Switching in a Nonlinear Periodic-Waveguide Structure," *Appl. Phys. Lett.* **60**, 1427 (1992).

24. N. D. Sankey, D. F. Prelewitz, T. G. Brown, and R. C. Tiberio, "Optical Switching Dynamics of the Nonlinear Bragg Reflector: Comparison of Theory and Experiment," *J. Appl. Phys.* **73**, 7111 (1993).

25. W. Luck, M. Klier and H. Wesslaw, "Kristallisation Ubermolekularer Bausteine," *Naturwissenschaften* **50**, 485 (1963).

26. P. A. Forsyth, S. Marcelja, D. J. Mitchell and B. W. Ninham, "Ordering in Colloidal Systems," *Adv. Colloid Interface Sci.* **9**, 37 (1978).

27. N. Ise, H. Matsuoka, K. Ito and H. Yoshida, "Colloidal Dispersions," *Faraday Discuss. Chem. Soc.* **90**, 153 (1990).

28. M. J. Moran, C. Y. She and R. L. Carmen, "Interferometric Measurements of the Nonlinear Refractive-Index Coefficient Relative to CS_2 in Laser-System-Related Materials," *IEEE J. Quantum Electron.* **QE-11**, 259 (1975).

29. P. St. J. Russell, "Bloch Wave Analysis of Dispersion and Pulse Propagation in Pure Distributed Feedback Structures," *J. Mod. Opt.* **38**, 1599 (1991).

30. C. L. Adler and N. M. Lawandy, "Optical Gradient Forces on Colloidal Crystals: Generation of Spatially Complex Structures," *Opt. Commun.* **91**, 354 (1992).

31. R. C. C. Leite, S. P. S. Porto and T. C. Damen, "The Thermal Lens Effect as a Power-Limiting Device," *Appl. Phys. Lett.* **10**, 100 (1967).

32. M. J. Soleau, W. E. Williams and E. W. VanStryland, "Optical Power Limiter with Picosecond Response Time," *IEEE J. Quantum Electron.* **QE-19**, 731 (1983).

33. E. Yablonovitch, "Photonic Band-Gap Structures," *J. Opt. Soc. Am. B* **10**, 283 (1993).

34. K. Ikeda, H Daido and O. Akimoto, "Optical Turbulence: Chaotic Behavior of Transmitted Light From a Ring Cavity," *Phys. Rev. Lett.* **45**, 709 (1980).

35. K. Ikeda, "Multiple-Valued Stationary State and Its Instability of the Transmitted Light by a Ring Cavity System," *Opt. Commun.* **30**, 257 (1979).

36. Y Silberberg and I. Bar Joseph, "Instabilities, Self-Oscillation, and Chaos in a Simple Nonlinear Optical Interaction," *Phys. Rev. Lett.* **48**, 1541 (1982).

37. R. L. Sutherland, V. P. Tondiglia, L. V. Natarajan, T. J. Bunning, and W. W. Adams, Electrically Switchable Volume Gratings in Polymer-Dispersed Liquid Crystals," *Appl. Phys. Lett.* **64**, 1074 (1994).

38. D. Whitney and R. T. Ingwall, "The Fabrication and Properties of Composite Holograms Recorded in DMP-128 Photopolymer," *Proc. of the SPIE* **1213**, 18 (1990).

39. R. T. Ingwall and T. Adams, "Hologram:Liquid Crystal Composites," *Proc. of the SPIE* **1555**, 279 (1991).

40. P. W. McOwan, M. S. Gordon, and W. J. Hossack, "A Switchable Liquid Crystal Binary Gabor Lens," *Opt. Commun.* **103**, 189 (1993).

41. M. Stalder and P. Ehbets, "Electrically Switchable Diffractive Optical Element for Image Processing," *Opt. Lett.* **19**, 1 (1994).

42. J. Zhang and M. B. Sponsler, "Switchable Liquid Crystalline Photopolymer Media for Holography," *J. Am. Chem, Soc.* **114**, 1506 (1992).

43. I. C. Khoo and Y. R. Shen, "Liquid Crystals: Nonlinear Optical Properties and Processes," *Opt.Eng.* **24**, 579 (1985).

44. S. D. Jacobs, " Liquid Crystal for Laser Applications," in *Handbook of Laser Science and Technology, Section 2: Special Properties,* Vol. IV, Part 2, pp. 409-465, edited by M. J. Weber (CRC Press, Boca Raton, FL, 1986).

45. R. Alferness, "Analysis of Optical Propagation in Thick Holographic Gratings," *Appl. Phys.* 7, 29 (1975).

46. T. Stone and N. George, "Wavelength Performance of Holographic Optical Elements," *Appl. Opt.* **24**, 3797 (1985).

DISTRIBUTION

AFSAA/SAI, Washington DC
AUL/LSE, Maxwell AFB, AL
DTIC/OCC, Alexandria, VA
PL/SUL/HO, Kirtland AFB, NM
Dr Michelle Malcuit, Lehigh University, Bethlehem, PA
Official Record Copy, (PL/LIDN, Dr Chris Clayton)